Equilibrium Response of an Atmosphere–Mixed Layer Ocean Model to Different Radiative Forcing Agents: Global and Zonal Mean Response

MASAKAZU YOSHIMORI AND ANTHONY J. BROCCOLI

Center for Environmental Prediction, and Department of Environmental Sciences, Rutgers, The State University of New Jersey, New Brunswick, New Jersey

(Manuscript received 2 August 2007, in final form 16 January 2008)

ABSTRACT

The equilibrium response to various forcing agents, including CO_2, solar irradiance, tropospheric ozone, black carbon, organic carbon, sulfate, and volcanic aerosols, is investigated using an atmospheric general circulation model coupled to a mixed layer ocean model. The experiments are carried out by altering each forcing agent separately. Realistic spatial patterns of forcing constituents are applied but the magnitude of the forcing is adjusted so that each forcing constituent yields approximately the same strength of radiative forcing. It is demonstrated that the global mean temperature response depends on the types of forcing agents and the efficacy with respect to CO_2 forcing ranges from 58% to 100%. The smallest efficacy is seen in one of the black carbon experiments and is associated with negative cloud feedback. The sign of the cloud feedback is shown to be sensitive to the vertical distribution of black carbon. The feedback analysis suggests that the small efficacy in tropospheric ozone is due to a large negative lapse rate feedback. Global mean precipitation increases when the earth warms except for the case of black carbon in which precipitation decreases. In all experiments, the global mean convective mass flux decreases when the earth's surface warms. When the applied radiative forcing resulting from a particular forcing agent is stronger in one hemisphere, anomalous heat exchange between the hemispheres results in conjunction with changes in the Hadley circulation. The magnitude of interhemispheric heat transport is little sensitive to the details of the forcing, but is determined primarily by the interhemispheric contrast in forcing. The change in the Hadley circulation strongly impacts the precipitation changes in low latitudes.

1. Introduction

The effect of elevated atmospheric carbon dioxide on climate has been a focus of many climate change studies. While CO_2 is the most important radiative forcing agent between the preindustrial period and the present day, contributions of other forcing agents are not negligible (e.g., Charlson et al. 1992; Haywood and Boucher 2000; Solomon et al. 2007; Hansen and Sato 2001; NRC 2005). In addition, it has been shown that climate sensitivity, defined here as the global and annual mean surface air temperature change per unit radiative forcing, depends on types of the forcing agent (Hansen et al. 1997a; Shine et al. 2003; Hansen et al. 2005; NRC 2005). Furthermore, the regional impact of spatially inhomogeneous constituents such as aerosols could be much larger than that implied by the global mean radiative forcing (Chung et al. 2002; Menon et al. 2002; Cheng et al. 2005; Shindell et al. 2006). Nevertheless, current understanding of the effect of non-CO_2 forcing on climate change is relatively poor.

Models used for climate change simulations are becoming more and more sophisticated, and detailed representation of various forcing constituents are being incorporated. In projections, detection, and attribution of climate change, it is essential that models accurately simulate both spatial patterns and amplitude of the response to external forcings. Although the evaluation of the accuracy is limited in comparisons with observations that result from a combined forcing of many agents, it is important to understand how models respond to different forcing agents. In attribution of climate change it is also fundamental that the climate system responds to one type of forcing agent differently from others.

The purpose of this study is to characterize some aspects of the quasi-equilibrium responses of a model to different radiative forcing agents and to provide a physical understanding of the responses. We aim to

Corresponding author address: Masakazu Yoshimori, Center for Climate System Research, University of Tokyo, 5-1-5, Kashiwanoha, Kashiwa-shi, Chiba, 277-8568, Japan.
E-mail: masakazu@ccsr.u-tokyo.ac.jp

DOI: 10.1175/2008JCLI2172.1

identify important processes that are responsible for the similarities and differences of the responses. In this paper, the annual mean response is presented with emphasis on global and zonal mean variables. The seasonal response with a more regional perspective will be presented elsewhere. The forcing agents include atmospheric CO_2 concentration, total solar irradiance, tropospheric ozone, black carbon, organic carbon, sulfate aerosols, and volcanic aerosols. While it is necessary to use the most comprehensive models, that is, coupled atmosphere–ocean general circulation models (GCMs), in formal projection, detection, and attribution studies, such models are computationally expensive. Consequently, integrations with only combined forcings are often conducted. As a complementary approach, we use an atmospheric GCM coupled with a mixed layer ocean model. The use of a mixed layer ocean model, rather than an ocean GCM, is a disadvantage for the purpose of realistic simulations because transient responses cannot be examined and the effect of ocean dynamics is not included. However, this approach has some advantages. The importance of "fast feedback" processes involving surface albedo, water vapor, and clouds can be readily assessed. In addition, a larger signal-to-noise ratio is expected because unforced low-frequency variability tends to be suppressed.

The outline of the rest of this paper is as follows. A brief description of the model is given in the next section, and the experimental design is described in section 3. Two analysis methods that are used to diagnose the results are explained in section 4. In section 5, results are presented in the order of global mean temperature, global mean precipitation, zonal mean temperature, and zonal mean precipitation changes. Summary and discussion are included in section 6.

2. Model description

The model used in this study is the NOAA Geophysical Fluid Dynamics Laboratory (GFDL) atmospheric GCM coupled to a mixed layer ocean model, which also includes land surface and sea ice components. The atmosphere, land surface, and sea ice model components are identical to those in the GFDL coupled climate model version 2.1 (CM2.1; Delworth et al. 2006). The CM2.1 was used, for example, for twentieth-century climate simulation (Knutson et al. 2006) and in future climate projections for the Intergovernmental Panel on Climate Change (IPCC) Fourth Assessment Report (AR4) (Solomon et al. 2007).

The atmospheric component is a primitive equation model with a finite volume dynamical core (Lin 2004). It has approximate horizontal resolution of 2.5° and 2.0° in longitude and latitude, respectively. The model has 24 hybrid sigma-pressure levels from about 30 m above the surface to about 3 hPa (~40 km) (GFDL GAMDT 2004). There are nine levels in the lowest 1.5 km above the surface and five levels in the stratosphere. Full radiation calculations are carried out every 3 h with a diurnal cycle. Aerosol species included are sulfate, organic carbon, black carbon, sea salt, and dust. The indirect effect of aerosols, a modification of cloud properties such as albedo and lifetime, is not included. There are three prognostic tracers associated with clouds: cloud liquid, cloud ice, and cloud fraction. The cloud microphysics and macrophysics are from Rotstayn (1997) and Tiedtke (1993), respectively, with a modification as described in Delworth et al. (2006). Moist convection is parameterized by the relaxed Arakawa–Schubert formulation (Moorthi and Suarez 1992).

The ocean component is represented by a 50-m-deep motionless mixed layer. To account for ocean heat transport, which is not represented by the model, heat flux anomalies are added to the ocean. This so-called q flux is determined so that the model produces realistic annual cycles of SST and sea ice. In the Southern Ocean, however, further adjustments are required due to model biases and the lack of dynamical ocean feedback: the model produces unrealistically large cooling in that region when a large but realistic negative radiative forcing is imposed. This problem is resolved by applying a zonal mean q flux to the south of 40°S with a smooth transition from zonally averaged to zonally varying q flux between 40° and 30°S, as in Jackson and Broccoli (2003). Note that runaway coolings with the use of slab ocean models were also reported by Mickley et al. (2004) in the Southern Ocean and Stainforth et al. (2005) in the eastern tropical Pacific. The q flux varies with season, but does not vary interannually or among the experiments conducted in this study.

The dynamic part of the sea ice component employs an elastic–viscous–plastic ice rheology, and predicts velocity of the ice pack and the area as described in Winton (2000). Since there are no ocean dynamics in the model, the sea ice is not affected by ocean currents. Thermodynamic properties of the ice pack are calculated for one snow layer with zero heat capacity and two ice layers in five categories of ice thickness distribution.

The land component assumes an isothermal surface for soil, snow, and vegetation within a grid cell, and has three reservoirs for water for unglaciated land—snowpack, root-zone water, and groundwater—and one

TABLE 1. A list of experiments: ΔC denotes the difference between 2000 and 1860 AD for the concentration of a radiatively active constituent indicated inside the parentheses.

Expt	Brief description
PI	Preindustrial control (1860 AD)
CO2	PI + increased carbon dioxide from 285.98 to 428.97 ppmv
SLR	PI + increased total solar irradiance from 1364.67 to 1376.50 W m^{-2}
TRO3	PI + 4.2 × ΔC(tropospheric ozone)
BC2W	PI + 3.3 × ΔC(black carbon)
OC	PI + 8.4 × ΔC(organic carbon)
SULF	PI + 2.2 × ΔC(sulfate aerosols)
VOLC	PI + 0.57 times the extinction optical depth due to volcanic aerosols in 1992
BC1W	PI + 1.6 × ΔC(black carbon)
BC2WLO	PI + 5.5 × ΔC(black carbon); the perturbation is imposed only below the $\sigma = 0.5$ level, i.e., lower troposphere

TABLE 2. Efficacy of forcing agents: ΔF is the global and annual mean instantaneous radiative forcing at the tropopause (W m^{-2}), ΔT the global and annual mean surface air temperature change (K), λ ($=\Delta T/\Delta F$) the climate sensitivity parameter (K W^{-1} m^2), and E the efficacy of forcing agents (see text for the definition of the efficacy).

Expt	ΔF	ΔT	λ	E
CO2	2.28	1.81	0.79	1.00
SLR	2.02	1.45	0.72	0.90
TRO3	2.00	1.02	0.51	0.65
BC2W	1.98	0.91	0.46	0.58
OC	−2.00	−1.21	0.60	0.76
SULF	−2.02	−1.59	0.79	0.99
VOLC	−2.01	−1.41	0.70	0.89
BC1W	0.99	0.46	0.47	0.59
BC2WLO	1.98	1.11	0.55	0.70

reservoir of snowpack for glaciated surface as described in Milly and Shmakin (2002).

A more detailed description of the atmosphere and land surface components is available in GFDL GAMDT (2004), and their minor modifications as well as the description of the sea ice component are available in Delworth et al. (2006).

3. Experimental design

We conducted nine idealized experiments with seven different radiative forcing agents in addition to a preindustrial (PI) simulation. All experiments are integrated at least 100 years and the last 50 years are analyzed, unless noted otherwise. The abbreviations for names of the experiments and their brief descriptions are summarized in Table 1. The PI simulation serves as a control case in our suite of experiments. The forcing of the PI control simulation is same as the corresponding coupled model simulation described in Delworth et al. (2006): all forcings are set for 1860 AD except for natural aerosols (sea salt and dust), which are prescribed based on the estimate for 1990 AD. The forcing includes seven different well-mixed greenhouse gases (GHGs), total solar irradiance, land cover type, anthropogenic aerosols (black carbon, organic carbon, and sulfate), and ozone. Note that exact values of well-mixed GHG concentrations are listed in Delworth et al. (2006, Table 1). The monthly mean, three-dimensional distributions of tropospheric ozone and aerosol concentrations are prescribed based on offline chemistry-transport model calculations (Horowitz et al. 2003). Black carbon and organic carbon contain both fossil fuel and biomass burning sources. Information on the input emission data for the offline chemistry-transport model is described in Delworth et al. (2006). The stratospheric ozone distributions were prescribed by zonal mean values based on observational studies (Randel and Wu 1999). Volcanic aerosols are not included in the PI control simulation.

There are two features in the experimental design: each forcing agent is applied separately in individual perturbation experiments, and the magnitude of the global and annual mean radiative forcing is approximately equal ($\sim\pm 2$ W m^{-2}) except for one perturbation experiment (BC1W; see also Table 2). Throughout this article, instantaneous radiative forcing, rather than adjusted radiative forcing, is used in describing the forcing in our experiments. This choice is simply for technical convenience. Indeed, the adjusted forcing has generally been favored as it represents the more effective forcing for the surface–troposphere system. The difference between the two forcings is on the order of 10% or less in most forcing agents considered here, but can be larger for tropospheric ozone (Berntsen et al. 1997; Hansen et al. 2005). Nevertheless, we do not think that the uncertainty arising from the use of the instantaneous forcing is as large as it would compromise the conclusions of this study.

The target strength of forcings is acquired by adjusting the concentration of the forcing agents iteratively in offline calculations using the radiation part of the GCM code. The radiative forcing is calculated using one year of three-hourly meteorological fields from the PI control simulation. In the SLR experiment, total solar irradiance is altered with equal fractional changes over the spectrum. Note that the inhomogeneous fractional change may influence the result to a minor extent (Hansen et al. 2005). The differences in tropospheric ozone, black carbon, organic carbon, and sulfate aero-

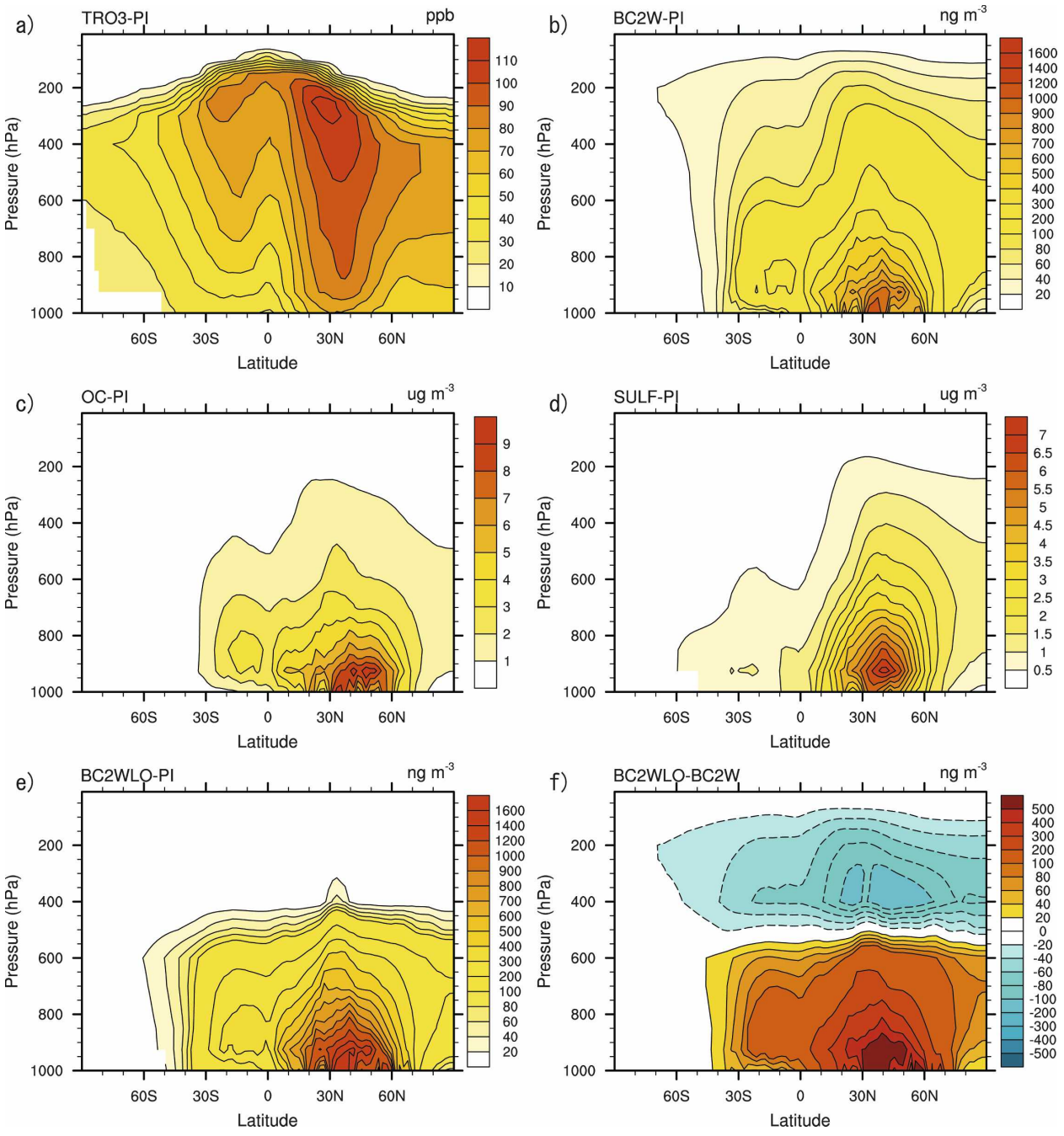

FIG. 1. Difference in ozone and aerosol concentrations, (a)–(e) from the PI control simulation and (f) from the BC2W experiment, imposed in the individual perturbation experiments: (a) tropospheric ozone in TRO3 (ppb), (b) black carbon in BC2W (ng m^{-3}), (c) organic carbon in OC (μg m^{-3}), (d) sulfate aerosols in SULF (μg m^{-3}), (e) black carbon in BC2WLO (ng m^{-3}), and (f) black carbon in BC2WLO (ng m^{-3}). Notice that the contours are not evenly spaced in black carbon concentrations (b), (e), and (f).

sol concentrations between years 2000 and 1860 are linearly amplified and added to the forcing of PI control simulation in the TRO3, BC2W, OC, and SULF experiments, respectively. The amplification factors differ between forcing agents. Zonal and annual mean perturbation concentrations in the TRO3, BC2W, OC, and SULF experiments are shown in Fig. 1. While perturbations in aerosol concentrations are mostly in midlatitudes and the lower troposphere, the largest perturbation in tropospheric ozone concentration is in relatively low latitudes and the upper troposphere. There is a substantial contrast in these perturbations between the

Northern and Southern Hemispheres. In the VOLC experiment, the effect of volcanic aerosols in 1992, the year of the peak negative radiative forcing due to the Mount Pinatubo eruption in June 1991, is added to the PI control simulation. The effect is represented by the extinction optical depth, single scattering albedo, and asymmetry factor in the model, and the extinction optical depth is reduced by 43%.

In addition to the BC2W experiment, two other experiments are designed for black carbon: BC1W and BC2WLO. In the BC1W experiment, the global mean radiative forcing is reduced to 1 W m^{-2}. The BC1W experiment aims to investigate the nonlinearity between the forcing and response. In the BC2WLO experiment, the black carbon concentration is modified only below the $\sigma = 0.5$ level, that is, lower troposphere, but still produces the same amount of the global mean radiative forcing as in the BC2W experiment. The amplification factor in BC2WLO experiment is required to be larger than BC2W experiment because the radiative forcing is larger when the absorbing aerosol is placed in higher altitude above reflective low clouds (Cook and Highwood 2004). The BC2WLO experiment aims to investigate the sensitivity of the response to vertical distribution of the black carbon, which is fairly uncertain. The perturbation concentration of black carbon in the BC2WLO experiment is shown in Figs. 1e and 1f as departures from the PI control and BC2W experiments, respectively.

After the completion of the integrations, we found that we had unintentionally introduced very small changes in the concentrations of background aerosols, that is, the aerosol species other than the forcing agent that was designed to be perturbed, with respect to the PI control simulation. Although the changes are less than 10^{-5} W m^{-2} in the global and annual mean and less than 10^{-3} W m^{-2} at any grid point, and thus are too small to have any practical importance, we conducted an additional control simulation that also introduced these very small changes in background aerosol concentrations. The new control simulation is integrated for another 80 years, and the last 50 years are used as a control case only for aerosol perturbation experiments. However, owing to the negligible difference between the two control simulations, we do not explicitly distinguish them in the following, and denote both as PI.

4. Analysis method

a. Partial radiative perturbation method

As a way to understand physical mechanisms of the surface temperature response to different forcing constituents, contributions of individual feedback processes are investigated (cf. Hansen et al. 1984; Schlesinger 1988). There are several different methods to evaluate the importance of individual feedback processes with each method having some advantages and disadvantages (e.g., Soden et al. 2004; Yokohata et al. 2005b,a; Bony et al. 2006; Soden and Held 2006; Taylor et al. 2007). We choose to use the so-called partial radiative perturbation (PRP) method pioneered by Wetherald and Manabe (1988) and applied to multiple models for an intercomparison study by Colman (2003). Since this method has been used repeatedly, only a brief description is given here.

If a forcing constituent is altered, net radiative imbalance or instantaneous radiative forcing at the tropopause results before the climate system adjusts to the perturbation. If a surface temperature change of ΔT_s results from a radiative forcing of ΔF, the climate sensitivity parameter is given by $\lambda = \Delta T_s/\Delta F$. In the equilibrium, the imposed radiative forcing is balanced by the change in net radiative flux caused by the adjusted climate system ΔR; that is, $\Delta F + \Delta R = 0$. The total feedback parameter $\hat{\lambda}$ is then defined as

$$\Delta F = -\Delta R = -\hat{\lambda}\Delta T_s. \tag{1}$$

Note that $\hat{\lambda} = -\lambda^{-1}$. If the contributions of nonlinear interactions between individual feedback processes to net radiative fluxes are ignored, that is, $\Delta R = \Sigma_i \Delta R_i$, the total feedback parameter is written as a sum of individual feedback parameters; that is, $\hat{\lambda} = \Sigma_i \hat{\lambda}_i$, where

$$\hat{\lambda}_i = \frac{\Delta R_i}{\Delta T_s}. \tag{2}$$

Here i represents ith feedback process. In the two-sided PRP feedback analysis, ΔR_i is estimated as follows:

$$\Delta R_i^{(0)} = R(x^{(0)}, \mu_i^{(1)}, \mu_{j\neq i}^{(0)}) - R(x^{(0)}, \mu_i^{(0)}, \mu_{j\neq i}^{(0)}), \tag{3a}$$

$$\Delta R_i^{(1)} = R(x^{(1)}, \mu_i^{(0)}, \mu_{j\neq i}^{(1)}) - R(x^{(1)}, \mu_i^{(1)}, \mu_{j\neq i}^{(1)}), \tag{3b}$$

$$\Delta R_i = [\Delta R_i^{(0)} - \Delta R_i^{(1)}]/2, \tag{3c}$$

where R is net radiative flux at the tropopause. Here superscripts (0) and (1) denote the control and perturbation experiments, respectively; x represents a forcing constituent such as CO_2; and μ_i represents meteorological fields that are associated with the ith feedback process. The actual computation is performed using the radiative transfer part of the GCM code. Water vapor, cloud, surface albedo, and total (surface + air) temperature feedbacks are calculated individually with this method. The total temperature feedback is further decomposed into the blackbody response and the lapse rate feedback. Here the blackbody response is defined as a radiative flux anomaly due to a hypothetical ho-

mogeneous temperature change for the entire atmosphere. It is crudely evaluated by adding the surface temperature change to the effective emission temperature and assuming blackbody radiation. The lapse rate feedback is then calculated as a residual of the blackbody response from the total temperature feedback.

While the PRP feedback analysis is generally a very valuable diagnostic tool, there are some limitations in our application: 1) the computation is conducted only for 5 years, rather than for entire 50 years, and thus the results are subject to sampling errors; 2) there could be nonlinear interactions between each feedback process, or inconsistencies between perturbed and reference meteorological fields that may introduce the so-called decorrelation errors (Colman and McAvaney 1997); 3) fast tropospheric adjustments not resulting from surface temperature change, such as cloud changes caused by aerosol changes, are evaluated as feedbacks (Shine et al. 2003; Lambert and Faull 2007); and 4) anomalous radiative fluxes at the tropopause do not necessarily scale to the surface air temperature changes. The last point requires some explanation. Suppose that feedback processes introduce the same amount of radiative flux at the tropopause at low and high latitudes. The resulting surface air temperature change in high latitudes could be much larger than in low latitudes. In a stratified atmosphere, the effects of the changes in surface fluxes induced by a radiative perturbation are concentrated in a relatively shallow layer rather than well distributed in the vertical, leading to a more intense near-surface response. Essentially, the PRP feedback analysis is a tool to evaluate radiative flux anomalies and not to directly evaluate surface temperature anomalies due to feedback processes. Nevertheless, it often provides valuable insight. Note that, unlike some previous studies, we evaluate the radiative flux at the tropopause, rather than top of the atmosphere, in order to link the feedback to the instantaneous forcing. The tropopause level is defined here as 100 hPa at the equator, descending linearly to 300 hPa at the poles.

b. Decomposition of moisture transport

The vertically integrated and zonally averaged moisture balance equation is given by

$$\frac{1}{g}\left\{\frac{\partial}{\partial t}\langle[q]\rangle + \frac{1}{a\cos\phi}\left\langle\frac{\partial[vq]\cos\phi}{\partial\phi}\right\rangle\right\} = [E - P], \quad (4)$$

where g is gravitational acceleration, t is time, q is specific humidity, and P and E are precipitation and evaporation rates, respectively. Also, $\langle A\rangle$ and $[A]$ denote vertical integration with respect to pressure and zonal average, respectively. In a statistical equilibrium, the tendency term may be ignored. Therefore, the difference in $P - E$ between two experiments is written as

$$\Delta[\overline{P} - \overline{E}] \approx -\frac{1}{g}\frac{1}{a\cos\phi}\left\langle\frac{\partial\Delta[\overline{vq}]\cos\phi}{\partial\phi}\right\rangle, \quad (5)$$

where $\overline{A}$ denotes average in time. For low latitudes, we can safely ignore the transient eddy component of the moisture transport (Peixoto and Oort 1992):

$$[\overline{vq}] = [\overline{v}][\overline{q}] + [\overline{v}^*\overline{q}^*] + [\overline{v'q'}] \approx [\overline{v}][\overline{q}] + [\overline{v}^*\overline{q}^*], \quad (6)$$

where A^* and A' denote deviations from the zonal and time averages, respectively. Consequently, the change in moisture transport is decomposed as

$$\Delta[\overline{vq}] = [\overline{v}]\Delta[\overline{q}] + [\overline{q}]\Delta[\overline{v}] + \Delta[\overline{v}]\Delta[\overline{q}] + \Delta[\overline{v}^*\overline{q}^*]. \quad (7)$$

Here the first term on the right-hand side represents the change in meridional moisture transport due to the change in specific humidity alone, the second term represents that due to the change in meridional circulation alone, the third term represents the covarying effect between the specific humidity and meridional circulation, and the last term represents the stationary eddy component. The decomposition is done with the monthly mean model output. Note that the same decomposition method was used in Yoshimori et al. (2006).

5. Results

a. Global mean temperature

In Solomon et al. (2007), the climate sensitivity obtained from equilibrium model calculations ranges from 2.1 to 4.4 K for a forcing of about 3.7 W m^{-2}, and was estimated between 2.0 and 4.5 K based on expert assessment. In addition, it was pointed out that the sensitivity to radiative forcing within the same model also depends on the types of forcing agents (e.g., Hansen et al. 1997a; Shine et al. 2003; Hansen et al. 2005). Hansen et al. (2005) termed the ratio of climate sensitivity for each forcing agent to that of CO_2 as the "efficacy." Note that the efficacy hereafter refers to the value evaluated with instantaneous radiative forcing unless otherwise noted explicitly. Note also that the cited values of efficacy from Hansen et al. (2005) have been adjusted by a factor of 0.9 for this comparison because their CO_2 efficacy with instantaneous radiative forcing is 90% of that with adjusted radiative forcing. Figure 2a shows the global mean temperature change per unit instantaneous radiative forcing in our individual forcing

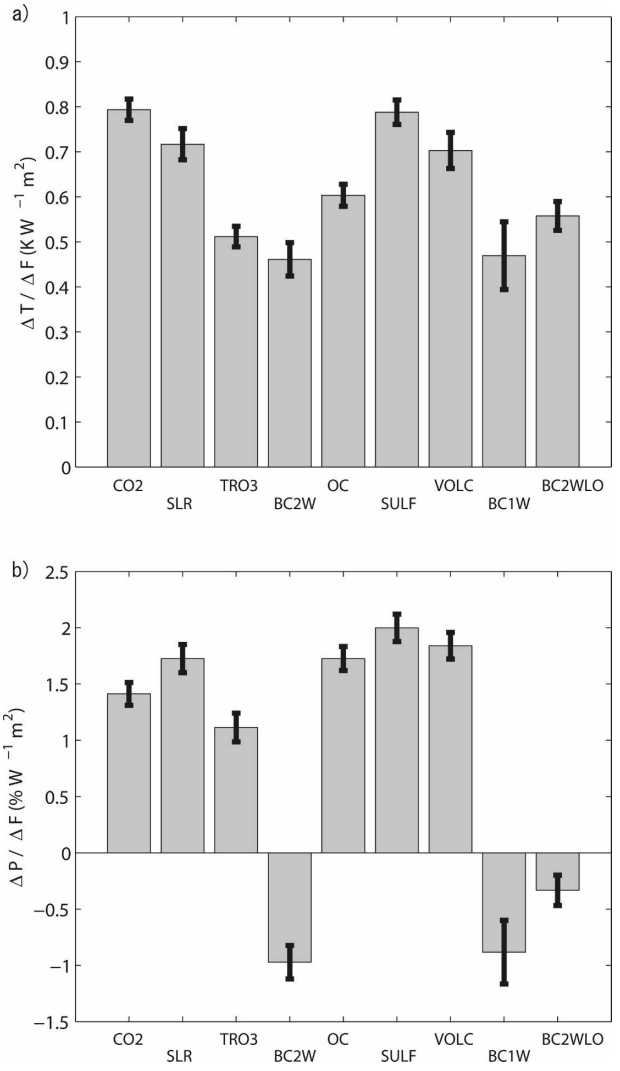

FIG. 2. Global and annual mean changes per unit instantaneous radiative forcing: (a) surface air temperature (K $W^{-1}m^2$) and (b) precipitation rate (% W^{-1} m^2). Vertical bars represent 5%–95% confidence intervals taking into account the interannual variability of surface air temperature and precipitation rate.

experiments. It varies over a range of sensitivities from about 0.46 K $(W m^{-2})^{-1}$ for black carbon to 0.79 K $(W m^{-2})^{-1}$ for CO_2 and sulfate aerosols. Thus, it depends, indeed, on the forcing agents.

Because the global mean temperature is an outcome of highly complicated interactions of feedback processes, it is extremely difficult to pin down the reasons for different efficacies without extensive sensitivity experiments for each forcing agent (cf. Hansen et al. 1997a, 2005). Such extensive experiments have not yet been carried out for this model. Here, we describe the results of our experiments in conjunction with other modeling studies to establish a general picture of the response. In addition, insight from the PRP feedback analysis is provided. It is, however, important to recall some of the limitations of the PRP method discussed in section 4 in assessing temperature response, and hence the interpretation from the feedback analysis should be taken as complementary. There are some differences in climate sensitivity parameter λ between Tables 2 and 3 because the latter values are calculated from only the five years of data used in the feedback analysis. In general, the sum of individual feedback parameters $\hat{\lambda}_{sum}$ and the total feedback parameter $\hat{\lambda}$ in Table 3 agree reasonably well. This ensures that the decorrelation errors are small, and the total feedback effect may be decomposed into and attributed to individual feedback processes.

The efficacy of solar forcing is estimated as 0.90 in our experiments (Table 2), meaning that solar forcing has a similar but slightly smaller potential in warming the earth's surface than CO_2 forcing with a given radiative forcing. This similarity has long been known (e.g., Manabe and Wetherald 1975; Wetherald and Manabe 1975). In an experiment with 2% increase of total solar irradiance, Hansen et al. (2005) estimated the efficacy of solar forcing as 1.10. On the other hand, Forster et al. (2000) found that the efficacy of solar forcing is about 0.85 with adjusted radiative forcing. The similarity of the sensitivity between CO_2 and solar forcing was described as "partly accidental" by Hansen et al. (1997a), which results from the tendency of higher sensitivity with more high-latitude forcing by CO_2 (Fig. 3a) and with more direct surface forcing by solar variations. In our experiments, the polar amplification by CO_2 forcing dominates (Fig. 3c). Note that radiative forcing is about 11% larger in CO2 than SLR experiments (Table 2). The feedback analysis, on the other hand, suggests that the slightly smaller efficacy of solar forcing is due to smaller cloud and albedo feedbacks although they are partly counteracted by the combined water vapor and lapse rate feedback (Table 3).

A general picture from previous studies that higher sensitivity results more high-latitude and more low-altitude forcing is qualitatively consistent with a relatively low efficacy of tropospheric ozone forcing of 0.65 in our experiments (Table 2). The forcing in this case is more concentrated toward low latitudes (Fig. 3a) and the upper troposphere. Note that Hansen et al. (2005) estimated the efficacy of tropospheric ozone as 0.76. The larger fractional forcing of tropospheric ozone in lower latitudes than CO_2 partly reflects the fact that the ozone change is more concentrated in low latitudes while CO_2 is uniformly distributed. It is also because absorption bands of ozone have less overlap than CO_2 with water vapor (Mickley et al. 2004). The higher sen-

TABLE 3. Feedback parameters estimated by the fluxes at the tropopause using the PRP method. Units are W m^{-2} K^{-1} except for λ, which has units of K (W m^{-2})$^{-1}$. Note that all feedback parameters in this table are calculated using the 5-yr meteorological fields in the integrations. The subscripts WV, C, A, and LR denote water vapor, cloud, (surface) albedo, and lapse rate feedbacks, respectively, and P denotes blackbody response: $\hat{\lambda}_{\rm sum}$ represents the linear sum of these feedback parameters while $\hat{\lambda}$ represents that calculated from the radiative forcing and surface air temperature response. Note that $\lambda = -\hat{\lambda}^{-1}$. The BC1W experiment is not included owing to low signal-to-noise ratio.

Expt	$\hat{\lambda}_{\rm WV}$	$\hat{\lambda}_C$	$\hat{\lambda}_A$	$\hat{\lambda}_P$	$\hat{\lambda}_{\rm LR}$	$\hat{\lambda}_{\rm WV+LR}$	$\hat{\lambda}_{\rm sum}$	$\hat{\lambda}$	λ
CO2	2.09	0.32	0.30	−3.34	−0.76	1.33	−1.39	−1.36	0.74
SLR	2.25	0.19	0.26	−3.41	−0.80	1.45	−1.51	−1.51	0.66
TRO3	1.91	0.38	0.18	−3.41	−1.09	0.81	−2.03	−2.10	0.48
BC2W	3.88	−1.02	0.22	−3.23	−1.99	1.89	−2.14	−2.10	0.48
OC	2.15	0.32	0.28	−3.44	−0.82	1.33	−1.52	−1.67	0.60
SULF	1.90	0.30	0.32	−3.38	−0.52	1.39	−1.38	−1.25	0.80
VOLC	1.94	0.61	0.34	−3.39	−0.65	1.29	−1.16	−1.25	0.80
BC2WLO	2.13	0.53	0.28	−3.14	−1.26	0.87	−1.46	−1.66	0.60

sitivity with more extratropical ozone forcing has been demonstrated by Joshi et al. (2003) and Stuber et al. (2001, 2005). It has also been shown that the efficacy is sensitive to the vertical distribution of ozone perturbations, and the perturbation in the upper troposphere tends to produce small efficacy (Joshi et al. 2003; Stuber et al. 2001, 2005). Mickley et al. (2004), however, found that there is little difference in efficacy between realis-

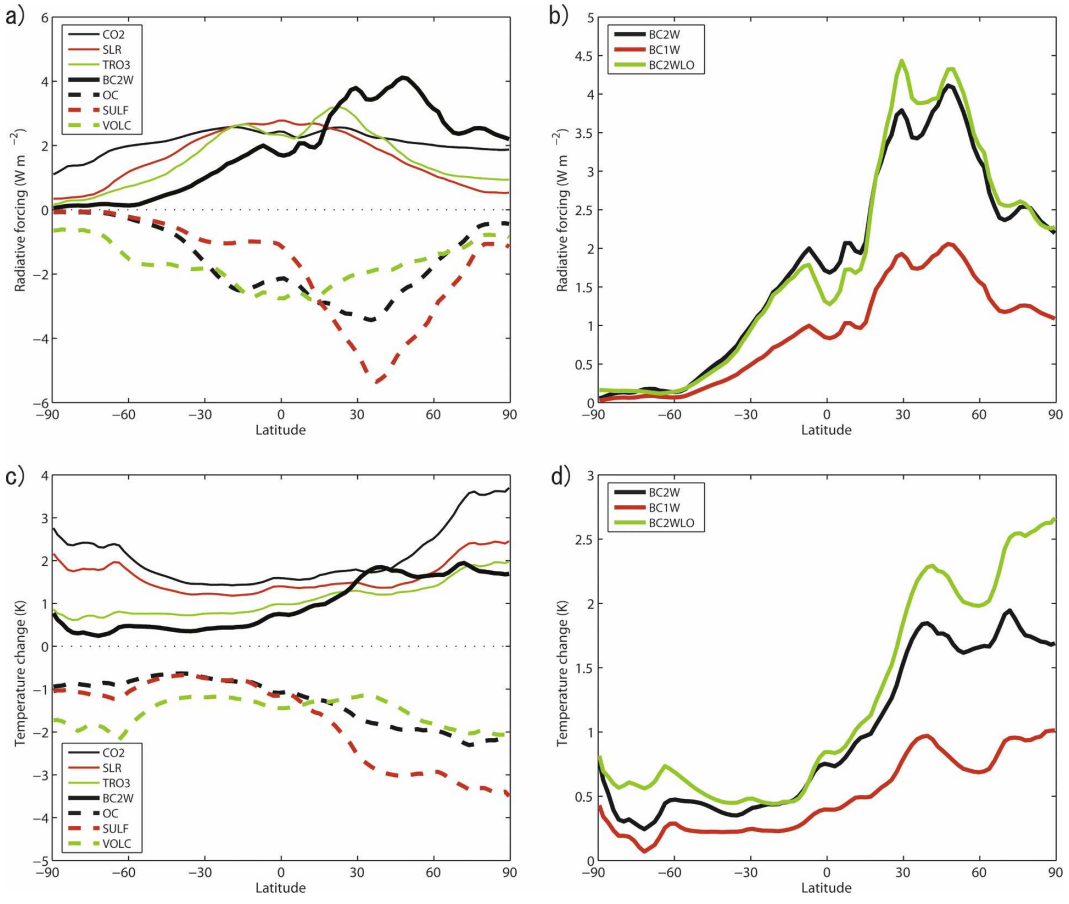

FIG. 3. Changes in zonal mean variables relative to the PI control simulation: (a) instantaneous radiative forcing at the tropopause (W m^{-2}) and (b) as in (a) but for black carbon experiments; (c) surface air temperature (K) and (d) as in (c) but for black carbon experiments.

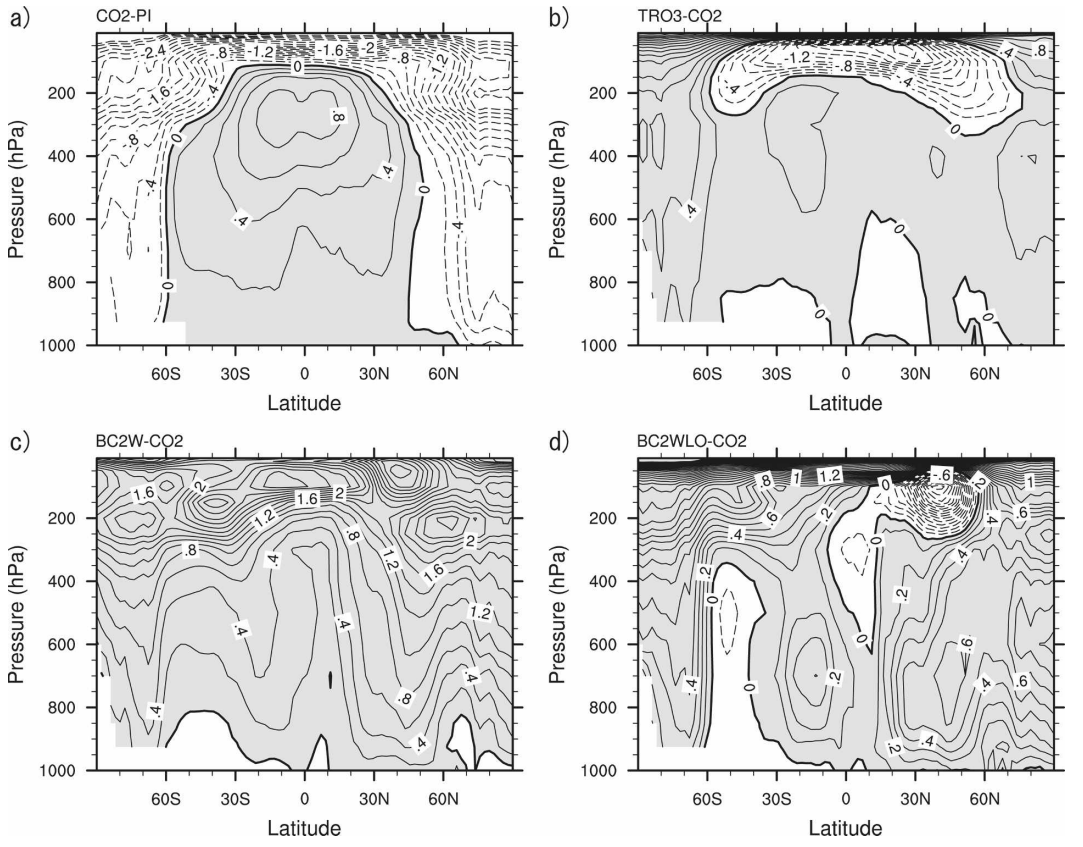

FIG. 4. Changes in thermal structure: $(\Delta T - \Delta T_s)/\Delta\overline{T}_{sa}$, where ΔT and ΔT_s are air and surface temperature changes, respectively, and $\Delta\overline{T}_{sa}$ is global mean surface air temperature change, with respect to the PI control simulation: (a) CO2, (b) TRO3-CO2, (c) BC2W-CO2, and (d) BC2WLO-CO2. Contour intervals are 0.2 and positive values are shaded.

tic and uniform distributions of tropospheric ozone change. They attributed the small efficacy of tropospheric ozone primarily to differences in vertical structure of the forcing, that is, midtropospheric forcing by CO_2 and upper-tropospheric forcing by ozone, which leads to a different cloud feedback. We also found that the increase of global mean cloud amount above 350 hPa and the decrease of low-level cloud amount by CO_2 forcing are larger than tropospheric ozone forcing. However, the feedback analysis shows a slightly larger positive cloud feedback in the TRO3 experiment, which does not account for its smaller efficacy. Instead, it suggests that more negative lapse rate feedback in the TRO3 experiment is responsible for its small efficacy (Table 3). Changes in the thermal structure support this interpretation (Figs. 4a and 4b). Joshi et al. (2003) also argues that an increased static stability reduces the coupling between upper troposphere and surface, which reduces the influence of warming in the upper troposphere on the surface.

The primary effect of two negative radiative forcing agents, organic carbon and sulfate aerosols, is a reduction of incident solar radiation at the surface through scattering in the atmosphere. Thus, the vertical distribution of these aerosols is unlikely an important factor for the difference in efficacy. The SULF experiment exhibits a stronger cooling in Northern Hemisphere mid and high latitudes than the OC experiment (Fig. 3c), and this difference is reflected in the efficacy. The stronger response in the SULF experiment in these regions is consistent with more extratropical forcing than the OC experiment (Fig. 3a). On the other hand, the difference in forcing strength in the Southern Hemisphere low latitudes between the two experiments is not reflected in local surface air temperature response. This might be due to the difference in land area between the two latitude bands over which the aerosols are most concentrated. In the feedback analysis, the largest difference between the two experiments is seen in the lapse rate feedback (Table 3). The larger negative lapse rate feedback in the OC experiment relative to the SULF experiment is due to the relatively larger

magnitude of forcing in the tropics where the temperature profile follows the moist adiabat. This result is consistent with Soden and Held (2006), who demonstrated a negative correlation between the lapse rate feedback and the ratio of tropical to global warming. However, the difference in lapse rate feedback is largely counteracted by the difference in water vapor feedback. The efficacy of organic carbon is relatively small in our estimate, which is in a large contrast to Hansen et al. (2005). They estimated that the efficacy of organic carbon due to fossil fuel combustion and biomass burning are 1.12 and 0.99, respectively. Our estimate of the efficacy for sulfate aerosols is also smaller than their estimates of 1.20.

Volcanic aerosols absorb both shortwave and longwave radiation in the stratosphere, reduce incident solar radiation at the surface, and produce negative radiative forcing at the tropopause. In contrast to the OC and SULF experiments, both radiative forcing and surface air temperature change are rather symmetric between the hemispheres, and exhibit roughly mirror images of the CO2 experiment with opposite signs (Fig. 3). In the feedback analysis, the VOLC experiment exhibits the largest positive cloud feedback (Table 3), which occurs mainly in low latitudes. In these latitudes, cloud amount decreases at about 100 hPa where strong warming and cooling occur above and below, respectively, and increases at about 300–400 hPa below that strong cooling. The quantitative link between these cloud changes and the cloud feedback strength remains to be explored, however. Our estimate of the efficacy for volcanic aerosols is close to the estimate of 0.93 in Hansen et al. (2005).

The smallest efficacy of 0.58 is found in the BC2W experiment (Table 2). This value is smaller than the efficacy of fossil fuel and biomass burning black carbon, 0.90 and 0.67, respectively, in Hansen et al. (2005). The efficacy of black carbon remains virtually unchanged when a weaker forcing is imposed in the BC1W experiment (see also Figs. 3b and 3d). The efficacy does change, however, when the vertical distribution of black carbon is varied in the BC2WLO experiment: more black carbon in the lower troposphere induces more near-surface warming (see also Figs. 3b and 3d). These results are qualitatively consistent with Roberts and Jones (2004), Hansen et al. (2005), and Sokolov (2006). In the feedback analysis, distinctly large negative lapse rate feedback is seen in the BC2W and BC2WLO experiments (Table 3 and Figs. 4c and 4d). It is, however, overcompensated by the large positive water vapor feedback in the former.

The feedback analysis also shows that cloud feedback is negative in the BC2W experiment while it is positive in the BC2WLO experiment (Table 3), indicating that the cloud feedback strongly depends on the vertical distribution of black carbon as shown in Sokolov (2006). The negative and positive cloud feedbacks in the BC2W and BC2WLO experiments occur primarily in shortwave and longwave fluxes, respectively. This is loosely consistent with the global mean cloud changes in which the BC2W experiment shows more high-level cloud reduction and less low-level cloud reduction than BC2WLO experiment. Figure 5 shows changes in cloud amount in the two black carbon experiments with the CO2 experiment for a reference. In the CO2 experiment, a qualitatively similar cloud change to Wetherald and Manabe (1988) is reproduced as a result that the thermal structure shifts upward near the tropopause. In the two black carbon experiments, asymmetric changes in cloud amount are seen between Northern and Southern Hemisphere low latitudes, which are consistent with changes in the Hadley circulation discussed in section 5d in detail. In the BC2W experiment, the increase in cloud amount in Northern Hemisphere midlatitudes seen in the CO2 and BC2WLO experiments is missing, and both BC2W and BC2WLO experiments show a reduction of cloud amount in the middle troposphere in Northern Hemisphere midlatitudes. The reduction of cloud amount in Northern Hemisphere midlatitudes is likely due to the result of direct local heating and a consequent reduction of relative humidity, the so-called semidirect effect of aerosols introduced by Hansen et al. (1997a). An increase of cloud amount in high latitudes in the BC2W experiment is probably associated with a decreased stability due to upper-tropospheric warming. Cook and Highwood (2004) also found that the climate sensitivity parameter is sensitive to single-scattering albedo of aerosols particularly when clouds are allowed to vary; global and annual mean cloud amount decreases linearly with single-scattering coalbedo of aerosols. Hansen et al. (1997a) found that the cloud feedback contributes to a surface warming with absorbing aerosols when distributed in model layers below the 720-hPa level, but contributes to a cooling when distributed below the 150-hPa level or between 550- and 250-hPa levels, loosely consistent with our results.

b. Global mean precipitation

In contrast to the global mean temperature, changes in global-mean hydrological cycle have been less extensively discussed. This is partly because the temperature response is generally more homogeneous than precipitation and considered more robust. Nevertheless, it is important that we also understand the global mean response of precipitation. Figure 2b shows changes in global mean precipitation rate per unit radiative forc-

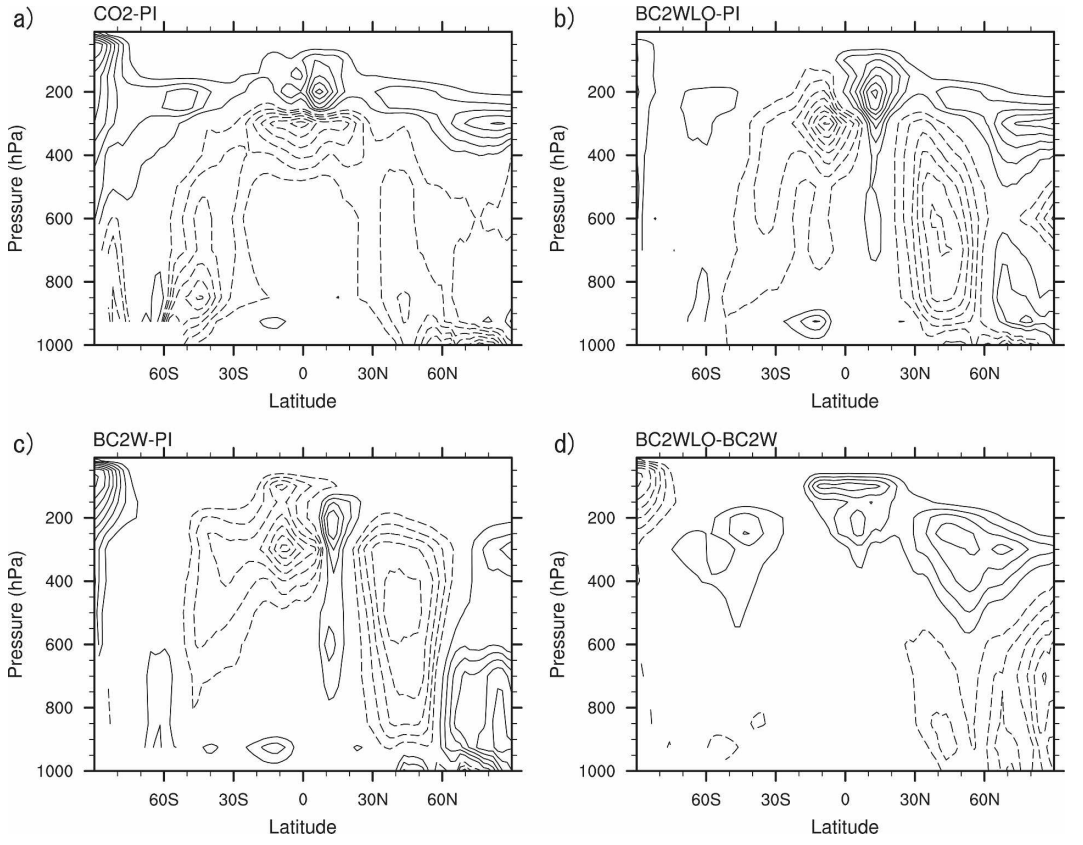

FIG. 5. Changes in cloud fraction: (a) CO2-PI, (b) BC2WLO-PI, (c) BC2W-PI, and (d) BC2WLO-BC2W. Contour intervals are 0.5%, and zero contours are omitted.

ing. Consistent with previous studies (Wang 2004; Hansen et al. 2005), the most striking result is that the precipitation rate decreases in the black carbon experiments even though the radiative forcing is positive and the global mean temperature increases (Fig. 2a). It is also seen, by comparing BC2W and BC2WLO, that the precipitation change depends on the vertical distribution of black carbon. Any nonlinearity in the precipitation response to between the BC2W and BC1W experiments cannot be ascertained due to internal variability, but it appears small.

The reduction of precipitation in black carbon experiments is reflected in the surface energy balance (Table 4). Although the radiative forcing at the tropopause is positive in both BC2W and BC2WLO experiments, the shortwave forcing at the surface is negative as a result of absorption by black carbon in the atmosphere. The net shortwave radiation at the surface relative to the PI control simulation remains negative (positive downward) in the equilibrium after the climate system is allowed to adjust. This reduction is partially balanced by the reduction of latent heat flux from the surface to the atmosphere and thus evaporation rate. In equilibrium, evaporation must be balanced by precipitation on the global average. This result agrees with the argument by Ramanathan et al. (2001) and the result by Cook and Highwood (2004), but it does not support Allen and Ingram (2002), who predict increased global mean precipitation with warming regardless of the forcing agent. Note that Roberts and Jones (2004) argue that their results are consistent with Allen and Ingram (2002).

While the analysis of the surface energy balance explains the sign of the response, it leaves the question as

TABLE 4. Global and annual mean surface energy fluxes in the three black carbon experiments (BC2W, BC1W, and BC2WLO) relative to the PI control simulation (W m^{-2}). SW, LW, LH, and SH denote shortwave, longwave, latent and sensible heat fluxes, respectively. Here the downward flux is defined as positive.

Expt	SW forcing	LW forcing	SW	LW	LH	SH
BC2W	−4.05	0.03	−4.83	1.85	1.61	1.29
BC1W	−2.00	0.01	−2.30	0.90	0.73	0.62
BC2WLO	−3.97	0.04	−3.97	1.53	0.55	1.81

to why the BC2WLO experiment shows about three times smaller reduction in the surface latent heat flux and precipitation than the BC2W experiment. Another way to look at the precipitation change is to investigate the heat budget in the atmosphere. It is well known that condensational heating is approximately balanced by dynamical and radiative coolings in the deep convective regions of the atmosphere. In subsidence regions, on the other hand, dynamical warming and radiative cooling are in approximate balance. In the global mean, in which horizontal heat transport may be ignored, the condensational heating is loosely balanced by the radiative cooling. The presence of radiative heating due to the absorption of shortwave radiation by black carbon in the atmosphere is balanced by a reduction in condensational heating compared to other forcing agents. This is particularly so in the lower troposphere where radiative damping is not efficient (Figs. 6a and 6b). There is more condensational heating in the upper troposphere in the BC2WLO than BC2W experiments (Fig. 6c). This corresponds to the lack of shortwave heating by black carbon in the upper troposphere in the BC2WLO experiment. It is of interest that the total precipitation changes in the black carbon experiments are dominated by decreased convective precipitation rather than increased large-scale precipitation (Table 5), consistent with Wang (2004). In all experiments, the large-scale precipitation increases as global temperature warms. The convective precipitation also shows the same tendency except for black carbon experiments.

Figures 7a and 7b show changes in precipitation rate and precipitable water per unit change in global-mean surface air temperature. While precipitation increases less than 2.9% K^{-1} and decreases in the black carbon experiments, precipitable water increases as much as 6.3 to 9.3 % K^{-1}. The magnitude of the precipitable water change is reasonably close to the value predicted by the Clausius–Clapeyron equation under the fixed relative humidity assumption (cf. Genfo et al. 1991; Held and Soden 2000; Wentz and Schabel 2000; Held and Soden 2006). As argued in previous studies (Betts and Ridgway 1989; Knutson and Manabe 1995; Held and Soden 2006), the larger fractional increase of storage (i.e., water vapor content) than flux (i.e., precipitation rate) implies that the residence time of water vapor in the atmosphere increases. In order for water vapor to remain in the atmosphere for a longer period of time, this in turn implies that the rate of exchange of water vapor between the planetary boundary layer and the free troposphere decreases. This is indeed the case for all forcing agents as represented here in convective mass flux at 500 hPa (Fig. 7c). A similar argument holds for convective mass flux changes in the tropics, and they are linked to vertical velocity changes (Fig. 8). Note that qualitatively similar changes in the vertical motion were reported for all IPCC AR4 models under the Special Report on Emissions Scenarios (SRES) A1B scenario by Held and Soden (2006) and Vecchi and Soden (2007).

It has been suggested that the tropical circulation involving vertical motion weakens on average when the earth's surface warms while it intensifies when the earth's surface cools (Zhang and Song 2006). Vecchi et al. (2006) extended this reasoning and demonstrated that the Walker circulation has been weakening over the last 130 years or so (see also Chen et al. 2002; Wielicki et al. 2002; Mitas and Clement 2005), and the trend is attributed to anthropogenic forcing based on coupled model simulations. We also find weaker east–west sea level pressure gradients in the CO2 and SLR warming experiments and a stronger gradient in the VOLC cooling experiment in which the meridional gradient in forcing is relatively small. The examination of velocity potential, however, exhibits a slightly more complicated picture (not shown). While the VOLC experiment exhibits an intensification of the Walker circulation, the response in the CO2 and SLR experiments is better described as a zonal displacement of the Walker circulation.

c. *Zonal mean temperature*

It has been demonstrated that thermal structure of the atmosphere is useful in distinguishing the responses to various radiative forcing agents (e.g., Santer et al. 1996; Tett et al. 1996). Figure 9 shows the vertical structure of zonal and annual mean air temperature changes relative to the PI control simulation. The stronger response in the upper troposphere compared to the lower troposphere is commonly seen in the deep tropics in all experiments. The signature of polar amplification is recognizable in most experiments, consistent with Fig. 3. A well-known feature of stratospheric cooling in the CO_2 experiment is simulated (e.g., Manabe and Wetherald 1967; Hartmann 1994, p. 332; Fig. 9a). A stratospheric cooling is also seen in the tropospheric ozone experiment (Fig. 9c), consistent with Mickley et al. (2004). This cooling is a result of increased opacity to upwelling longwave radiation in the troposphere. On the other hand, a stratospheric warming occurs in the volcanic experiment due to the absorption of shortwave and longwave radiation by volcanic aerosols (Fig. 9g), qualitatively consistent with Stenchikov et al. (1998). The enhanced response in midlatitudes in the BC2W, OC, and SULF experiments corresponds to the increased aerosol concentrations in those latitudinal

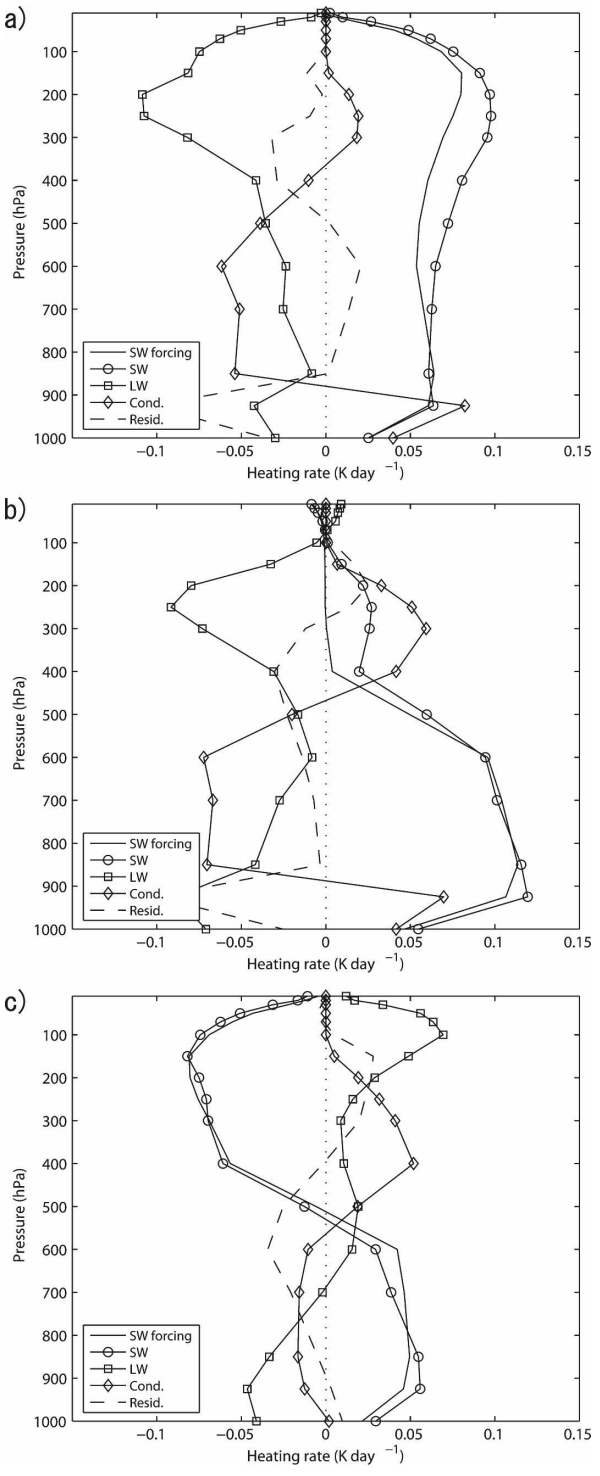

FIG. 6. Vertical profiles of global and annual mean variables relative to the PI control simulation: (a) heating rate for forcing and equilibrium in the BC2W experiment (K day^{-1}), (b) heating rate for forcing and equilibrium in the BC2WLO experiment (K day^{-1}), and (c) the difference in heating rate between BC2W and BC2WLO experiments (K day^{-1}). "SW," "LW," "Cond.," and "Resid." denote shortwave, longwave, and condensational heating rates, and residuals, respectively.

TABLE 5. Global and annual mean changes in total, large-scale, and convective precipitation relative to the PI control simulation (mm yr^{-1}). The fractional changes of the corresponding variables from the PI control simulation are also shown inside the parentheses. All values are statistically significant at 1% level of falsely rejecting the null hypothesis.

Expt	Total	Large-scale	Convective
CO2	33.7 (3.2%)	22.2 (8.2%)	11.6 (1.5%)
SLR	36.6 (3.5%)	21.6 (7.9%)	15.0 (1.9%)
TRO3	23.4 (2.2%)	15.5 (5.7%)	7.9 (1.0%)
BC2W	−20.2 (−1.9%)	11.5 (4.2%)	−31.7 (−4.1%)
OC	−36.3 (−3.5%)	−15.3 (−5.6%)	−21.0 (−2.7%)
SULF	−42.4 (−4.0%)	−14.3 (−5.3%)	−28.1 (−3.6%)
VOLC	−38.8 (−3.7%)	−14.7 (−5.4%)	−24.1 (−3.1%)
BC1W	−9.2 (−0.9%)	5.3 (2.0%)	−14.5 (−1.9%)
BC2WLO	−6.9 (−0.7%)	13.0 (4.8%)	−20.0 (−2.6%)

bands. In the BC2W experiment, the warming occurs in the upper troposphere while a relatively uniform vertical warming occurs in the BC2WLO experiment. The BC1W experiment shows a very similar structure of warming to the BC2W experiment (not shown).

Figure 10 shows zonal mean zonal wind changes relative to the PI control simulation. The strong warming in the upper troposphere leads to strengthened subtropical jets in the CO2, SLR, and VOLC experiments. In the Northern Hemisphere, the westerlies show meridional displacement in other experiments, particularly in the BC2W, SULF, and BC2WLO experiments. These shifts are consistent with the midlatitude temperature changes associated with aerosol concentrations there in which a warming in midlatitudes drives stronger and weaker jets in the north and the south, respectively.

d. Zonal mean precipitation

Changes in zonal mean precipitation rate exhibit remarkably different meridional structures between forcing agents (Fig. 11a). In high latitudes around 60° in both hemispheres, increased and decreased precipitation are seen in the warming and cooling experiments, respectively. This suggests that at least the sign of the zonal mean precipitation change in these latitudes is associated with the global-scale temperature change and thus the sign of radiative forcing at the tropopause. It is well known that the poleward transport of moisture increases with increased atmospheric water vapor content under warming (Fig. 7b). In low latitudes, changes in precipitation are more complicated: the CO2, SLR, and TRO3 experiments show an overall increase with a small decrease between about 10° and 20°S. On the other hand, the VOLC experiment shows an overall decrease with a small increase between 10° and 30° in both hemispheres. Three black carbon experiments ex-

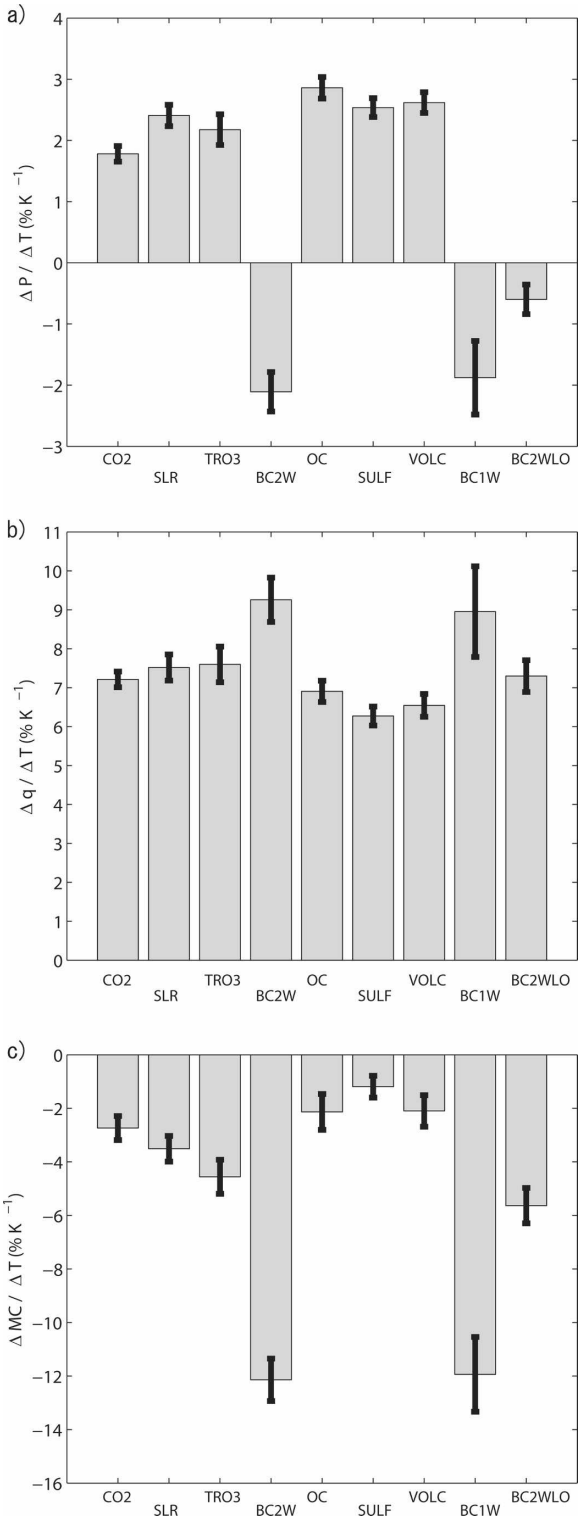

FIG. 7. Global and annual mean fractional changes per unit surface air temperature change: (a) precipitation rate, (b) precipitable water, and (c) convective mass flux at 500 hPa. Vertical bars represent 5%–95% confidence intervals taking into account the interannual variability of precipitation rate, precipitable water, and convective mass flux.

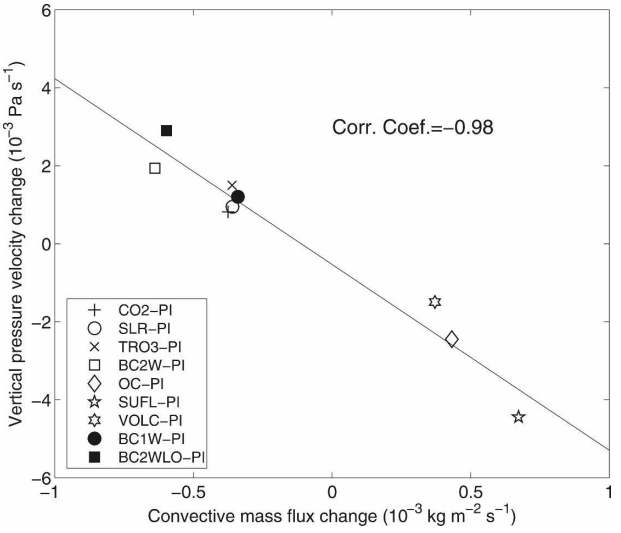

FIG. 8. The relation between convective mass flux and vertical pressure velocity changes in the tropics (30°S–30°N). Both variables are averaged over regions where the convective mass flux decreases (increases) with global-mean surface warming (cooling), i.e., $\Delta MC/\Delta T < 0$ (cf. Fig. 7c).

hibit precipitation increases and decreases in Northern and Southern Hemisphere low latitudes, respectively (not shown, but see Fig. 11d). In contrast, the OC and SULF experiments exhibit decreases and increases in Northern and Southern Hemisphere low latitudes, respectively. The peak changes occur around 10° in both hemispheres in these five aerosol experiments.

While changes in global-mean precipitation rate are balanced by changes in global-mean evaporation rate, the meridional structure in precipitation changes is not reflected in evaporation changes (Fig. 11b). In comparison with precipitation, changes in zonal mean evaporation occur relatively uniformly over the globe except for very high latitudes where the surface is covered by snow or ice. Except for black carbon experiments, evaporation rate increases and decreases in the warming and cooling experiments, respectively. It is therefore obvious that zonal mean precipitation change is primarily determined by the convergence and divergence of meridional moisture transport (Figs. 11c and 11d).

The transport of moisture is determined by two factors: circulation and amount of moisture in the atmosphere. To determine whether changes in moisture transport are caused by changes in either or both of these two factors, the convergence of meridional moisture transport is diagnosed by decomposing it into four contributions as described in section 4b: 1) zonal mean humidity change alone, denoted by $[v]\Delta[q]$; 2) meridional circulation change alone, denoted by $[q]\Delta[v]$; 3)

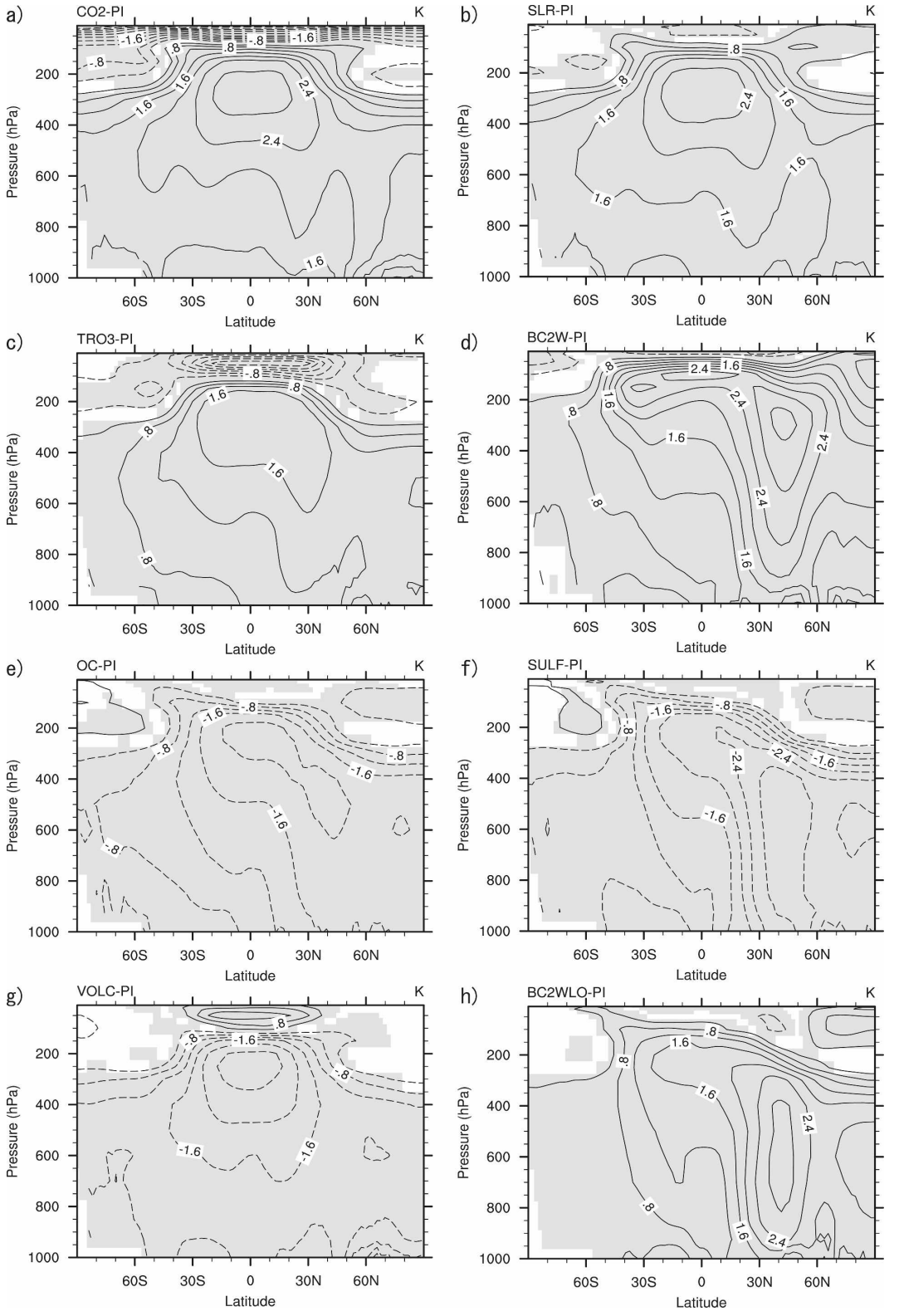

FIG. 9. Zonal mean air temperature changes relative to the PI control simulation: (a) CO2, (b) SLR, (c) TRO3, (d) BC2W, (e) OC, (f) SULF, (g) VOLC, and (h) BC2WLO experiments. Shadings represent that the difference is statistically significant at 1% level. Contour intervals are 0.4 K, and zero contours are omitted.

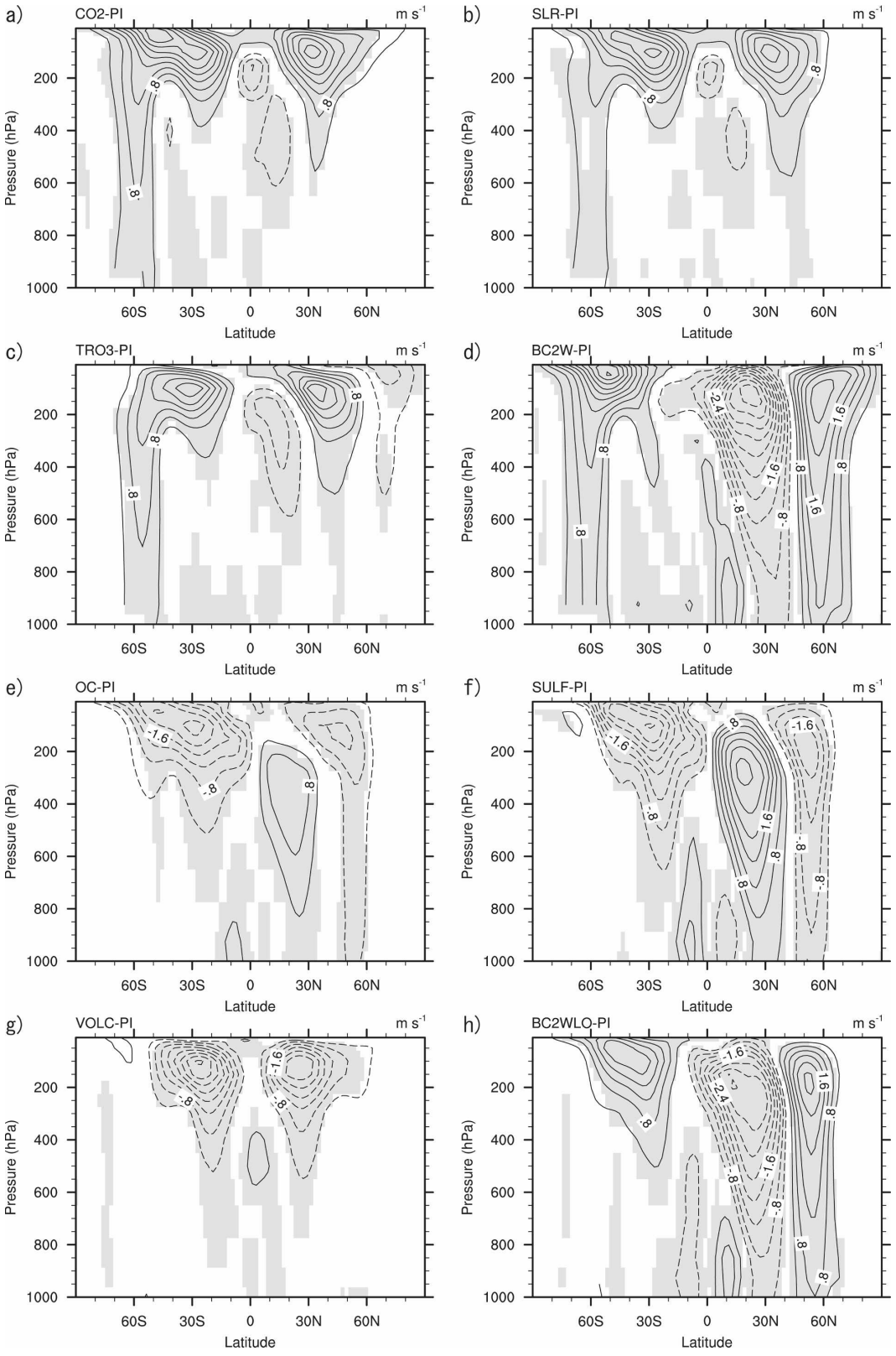

FIG. 10. As in Fig. 9 but for zonal mean zonal wind changes. Contour intervals are 0.4 m s^{-1} and zero contours are omitted.

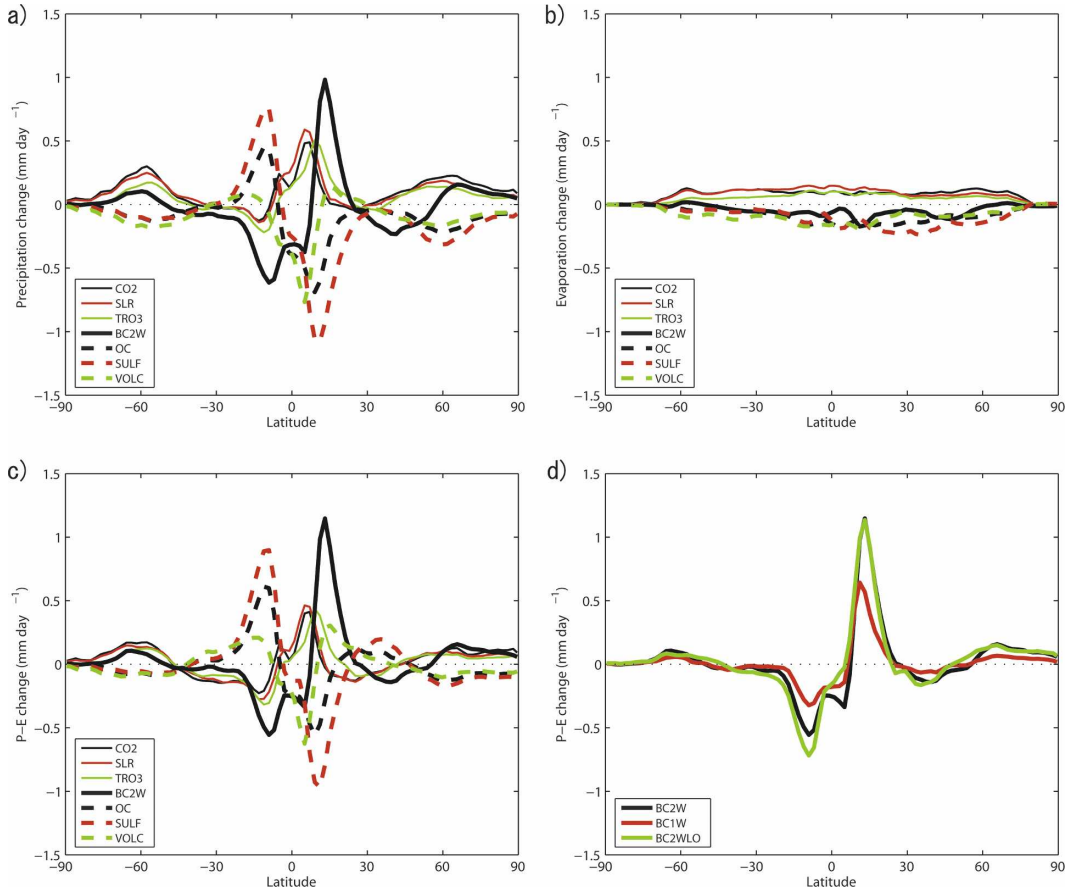

FIG. 11. Zonal and annual mean changes relative to the PI control simulation: (a) precipitation rate (P), (b) evaporation rate (E), (c) $P - E$, and (d) $P - E$ for black carbon experiments.

covariation of the two, denoted by $\Delta[v]\Delta[q]$; and 4) stationary eddies, denoted by $\Delta[v^*q^*]$. Figure 12 shows the results of the decomposition in individual forcing experiments with respect to the PI control simulation. In all analyses, the change in precipitation minus evaporation ($P - E$) is satisfactorily reproduced by the convergence of meridional moisture transport calculated by monthly mean specific humidity and meridional wind velocity denoted by $\Delta[vq]$. This supports the reliability of the analysis. In all cases, the covariance and stationary eddy contributions are relatively small and are not important. In the CO2 experiment, the increase of precipitation in low latitudes is dominated by the contribution of specific humidity change. In the SLR and TRO3 experiments, the effect of specific humidity change is comparable to the effect of circulation change in Northern Hemisphere low latitudes. For the rest of the experiments, the contribution of specific humidity change is secondary compared to the contribution of circulation change. Therefore, it is important to understand the change in the Hadley circulation in order to understand the zonal-mean precipitation changes in low latitudes.

Figure 13 shows changes in annual-mean meridional overturning mass streamfunction between 40°S and 40°N in individual forcing experiments with respect to the PI control simulation. Except for the CO2 and VOLC experiments, there is a distinct monopole pattern that may be described as an anomalous cross-equatorial Hadley circulation. In a broader context, previous modeling studies have shown similar Hadley circulation changes in response to various external forcings: Broccoli (2000), Chiang et al. (2003), and Chiang and Bitz (2005) in simulations of the Last Glacial Maximum; Vellinga and Wood (2002), Dahl et al. (2005), and Zhang and Delworth (2005) in the so-called water hosing experiments; Ramaswamy and Chen (1997) in the experiments with GHGs and surface albedo forcing; Williams et al. (2001) and Rotstayn and Lohmann (2002) due to indirect effect of aerosols; Wang (2004) by black carbon; and Broccoli et al. (2006) in an idealized experiment. These modeling studies as well as

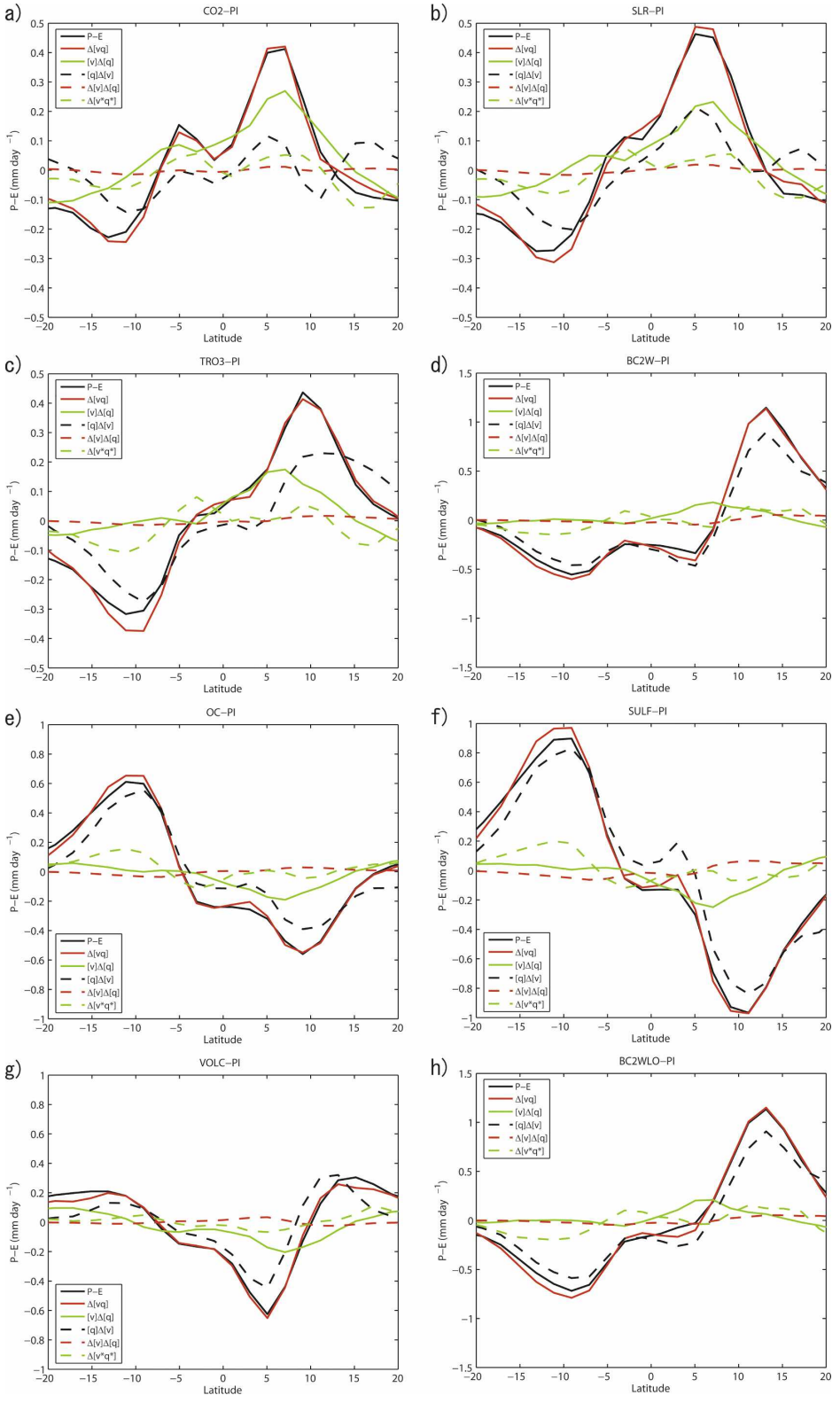

FIG. 12. Decomposition of moisture transport changes from the PI control simulation into terms of specific humidity change (green solid), circulation change (black dashed), covariance of the specific humidity and circulation (red dashed), and stationary eddy change (green dashed) (mm day^{-1}): (a) CO2, (b) SLR, (c) TRO3, (d) BC2W, (e) OC, (f) SULF, (g) VOLC, and (h) BC2WLO experiments.

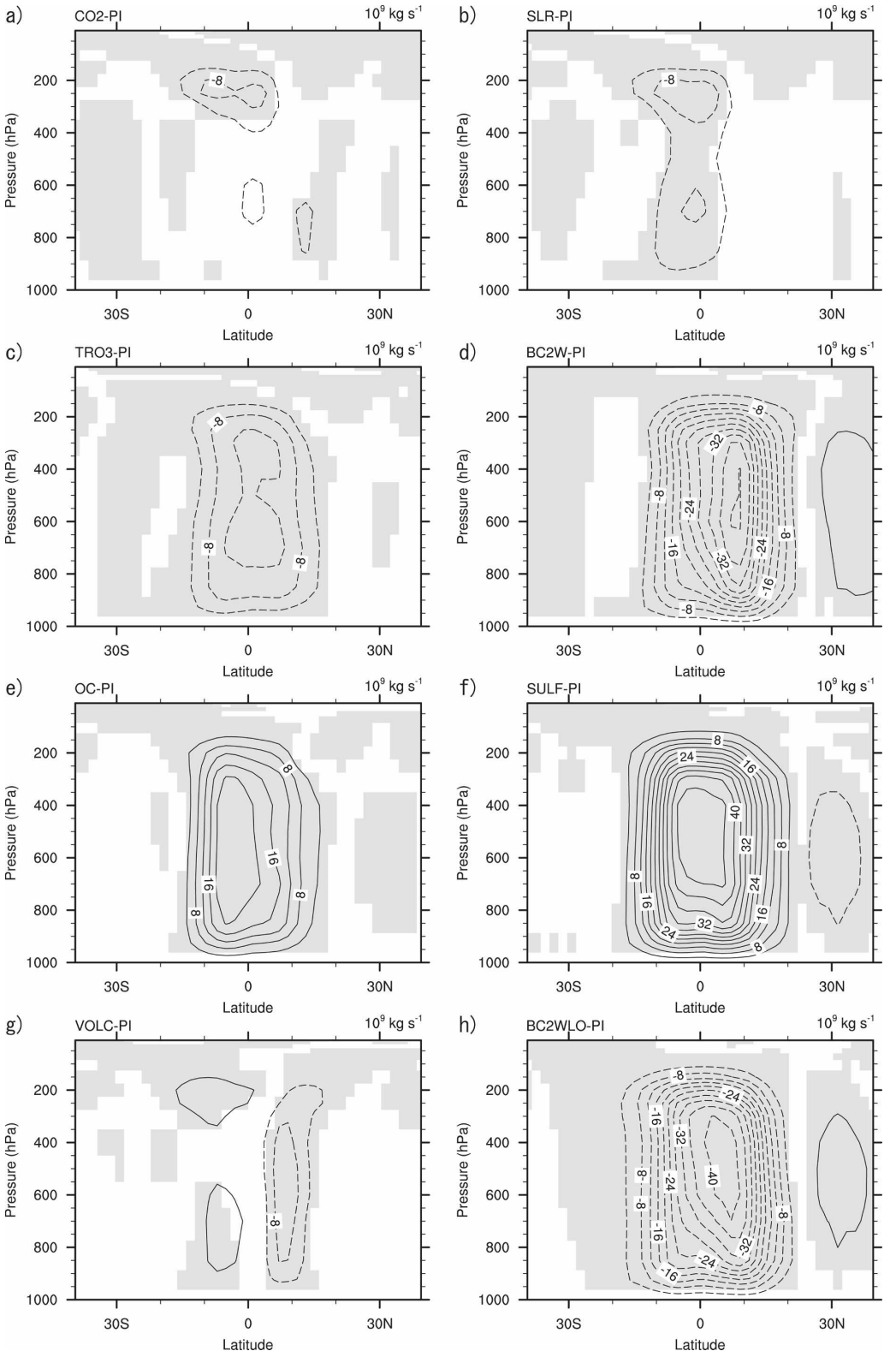

FIG. 13. Changes in zonally integrated mass streamfunction relative to the PI control simulation: (a) CO2, (b) SLR, (c) TRO3, (d) BC2W, (e) OC, (f) SULF, (g) VOLC, and (h) BC2WLO experiments. Positive (negative) values indicate clockwise (counterclockwise) circulation anomalies. Shadings represent that the difference is statistically significant at 1% level. Contour intervals are 4×10^9 kg s^{-1} and zero contours are omitted.

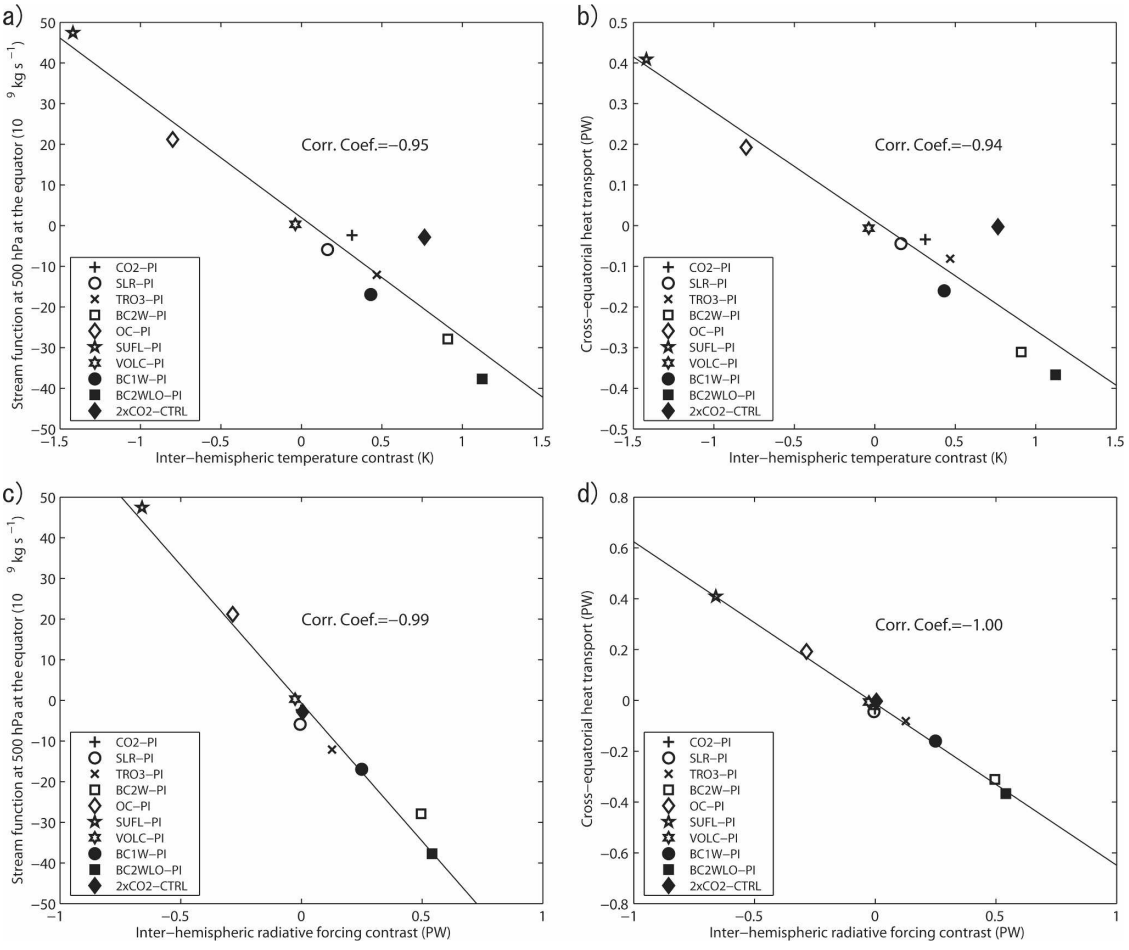

FIG. 14. Correlation analysis on the Hadley circulation changes: (a) interhemispheric temperature contrast and the Hadley circulation index, (b) interhemispheric temperature contrast and the cross-equatorial heat transport, (c) interhemispheric radiative forcing contrast and the Hadley circulation index, and (d) interhemispheric radiative forcing contrast and the cross-equatorial heat transport. Here interhemispheric temperature contrast is defined by the difference between Northern Hemisphere average and Southern Hemisphere average temperatures. On the other hand, interhemispheric radiative forcing contrast is defined as the difference between the Northern Hemisphere integrated and Southern Hemisphere integrated radiative forcings. Also, the Hadley circulation index represents the value of meridional mass streamfunction at the equator and 500-hPa level. Note that 1 PW of total energy flux is approximately equivalent to 4 W m^{-2} of energy fluxes when distributed uniformly over a single hemisphere. Note also that "CO2-PI" is superposed by "2×CO2 − CTRL" in (c) and (d).

some paleo-proxy records consistently suggest that the ascending branch of the Hadley circulation tends to become stronger in the hemisphere with more warming or less cooling, and weaker in the hemisphere with less warming or more cooling. To quantify and summarize the results in our experiments, we investigate a relation between the interhemispheric temperature contrast and the Hadley circulation changes. For convenience, we define the Hadley circulation index as a value of meridional mass streamfunction at 500 hPa at the equator. Thus, positive values of the Hadley circulation index indicate that the anomalous Hadley circulation has an ascending branch in the Southern Hemisphere and a descending branch in the Northern Hemisphere.

Figure 14a shows a scatterplot of interhemispheric temperature contrast and the Hadley circulation index. Here, the interhemispheric temperature contrast is defined simply as the difference in hemispheric average near-surface air temperature between the Northern and Southern Hemispheres. In addition to the experiments listed in Table 1, the CO_2 doubling experiment with respect to 1990 present-day simulation, denoted as "2×CO2 − CTRL," is added. The forcing used in our experiments yield interhemispheric temperature contrast ranging from about −1.5 to 1.5 K. In each figure,

there is a fairly high correlation between the two variables investigated. When the Northern Hemisphere undergoes greater warming than the Southern Hemisphere, the anomalous cross-equatorial Hadley circulation with the ascending branch in the Northern Hemisphere develops. When the Northern Hemisphere undergoes greater cooling than the Southern Hemisphere, an opposite pattern of the anomalous Hadley circulation develops. The strength of the Hadley circulation and the heat transport changes are highly correlated; the correlation coefficient between the Hadley circulation index and cross-equatorial heat transport is 0.99 in our experiments. There is also a good correlation between the interhemispheric temperature contrast and the northward heat transport at the equator (Fig. 14b). This relation is consistent with the interpretation that anomalous heat is transported from the warmed to the cooled hemisphere in Broccoli et al. (2006).

A careful inspection of the relation between the interhemispheric temperature contrast and the cross-equatorial heat transport changes, however, finds an obvious outlier, that is, 2×CO2 − CTRL in Figs. 14a and 14b. Note that this was first pointed out by Held and Soden (2006). As the Hadley circulation is closely related to the meridional heat transport, and thus to net radiation at the top of the atmosphere, it is natural to wonder if there may be a better relation between radiative forcing and the changes in the Hadley circulation. Figure 14c shows the scatterplot between the interhemispheric radiative forcing contrast and the Hadley circulation index, while Fig. 14d shows the relation between the interhemispheric radiative forcing contrast and the cross-equatorial heat transport changes. Here the interhemispheric radiative forcing contrast is defined as the difference in the integrated radiative forcing between Northern and Southern Hemispheres. In each figure, there is an even better correlation than when we used interhemispheric temperature contrast. When the same amount of radiative forcing is imposed on each hemisphere, equilibrium is achieved without changes in net heat transport between the hemispheres. On the other hand, when the radiative forcing is stronger in one hemisphere, an anomalous heat exchange between the hemispheres results. This heat exchange is accomplished by an anomalous cross-equatorial Hadley circulation, with the ascending branch in the hemisphere with a more positive or less negative radiative forcing and the descending branch in the hemisphere with a less positive or more negative radiative forcing.

As the ascending branch of the Hadley cell is accompanied by low-level mass convergence, the mean latitude of the ITCZ moves toward the hemisphere with the more positive or less negative radiative forcing in the annual mean. Because the hemisphere with the more positive radiative forcing typically undergoes greater warming, the ITCZ usually, but not always, appears to move toward the warmer hemisphere. The clockwise cross-equatorial Hadley circulation anomaly is accompanied by an increase and a decrease of precipitation in the southern and northern tropics, respectively. The opposite is true for the counterclockwise circulation anomaly. Figure 14d also shows that about 60% of the integrated radiative forcing contrast is compensated by an anomalous heat exchange between the hemispheres via the change in the Hadley circulation. The amount of energy transported interhemispherically is probably determined by a result of various feedback processes, the details of which are beyond the scope of this paper.

6. Summary and discussion

The equilibrium response of an atmosphere–mixed layer ocean model to various radiative forcing agents is investigated. The forcing agents include CO_2, total solar irradiance, tropospheric ozone, black carbon, organic carbon, sulfate, and volcanic aerosols. Experiments are carried out with an amplified magnitude of forcing yet retaining the realistic spatial patterns of ozone and aerosol changes from the preindustrial period to the present.

It is demonstrated that the global mean temperature response depends on the forcing agents. Tropospheric ozone and black carbon show distinctly smaller efficacy relative to CO_2, qualitatively consistent with previous studies. For black carbon, the efficacy can be as small as 0.58. The feedback analysis suggests that the small efficacy of black carbon is due to large negative cloud feedbacks. It is shown, however, that the sign of cloud feedback depends on the vertical distribution of black carbon. Any nonlinearity in the response to black carbon forcing is not clearly distinguishable from the interannual variability, but it appears small. The feedback analysis also suggests that the small efficacy of tropospheric ozone is due to a large negative lapse rate feedback. It should be noted that the definition of the tropopause will likely affect the details of the feedback analysis result, particularly in the longwave component, although the main conclusion should still hold. For a more quantitatively accurate assessment and future studies, the use of adjusted radiative forcing and the evaluation of radiative fluxes at the top of the atmosphere in the feedback analysis may be preferred.

Although the feedback analysis, which aims to evaluate the radiative flux at the tropopause, does not reveal

an important contribution of surface albedo feedback to variations in efficacy, the experiments with high efficacy generally exhibit a large high-latitude temperature change. For the general tendency of higher efficacy with high-latitude forcing, at least three explanations have been proposed: 1) stronger stratification in high-latitude atmosphere (Manabe and Wetherald 1975; Forster et al. 2000); 2) larger surface albedo feedback to high-latitude forcing (Hansen et al. 1997a; Stuber et al. 2005); and 3) nonlinear dependence of radiative damping on emission temperature (Joshi et al. 2003). For the general tendency of higher efficacy with low-altitude forcing, on the other hand, at least two explanations have been given: 1) stronger coupling with the surface (Hansen et al. 1997b), and upper-tropospheric positive forcing tends to increase stability and thus further reduces the coupling with the surface (Joshi et al. 2003); and 2) near-surface positive forcing tends to reduce low-level cloud (Hansen et al. 1997b; Cook and Highwood 2004). The quantification of the effect of each feedback process on surface temperature change needs to be explored further in the future.

In comparison with other studies, there seems to be variations in efficacy for certain forcing constituents. The current use of different distributions of forcing constituents prohibits the investigation of the reasons for these variations. One possibility is that the differences in the strengths of various feedbacks among models contribute to the variations in efficacy. For example, a forcing that is concentrated at high latitudes may lead to a higher efficacy in a model that has a strong albedo feedback than in a model with a weak albedo feedback. Nevertheless, the intermodel spread in CO_2 climate sensitivity is larger and still remains a large source of uncertainty in the response of future climate to anthropogenic forcing.

Global mean precipitation increases when the earth's surface warms except in the case of forcing by black carbon. The reduction of global mean precipitation by black carbon is consistent with the surface energy balance and atmospheric thermodynamic energy budget. In all experiments, global and tropical mean convective mass flux decreases when the earth's surface warms. In previous studies, this led to a notion of a weaker tropical overturning circulation, particularly the Walker circulation, when the earth warms. While the Walker circulation becomes stronger in the volcanic aerosol experiment, it is better described as zonally displaced in our CO_2 and solar irradiance experiments.

It is shown that tropical precipitation, meridional ITCZ displacement, and Hadley circulation are correlated with the interhemispheric temperature contrast as in many previous studies. In the present study, it is demonstrated that they are even more tightly linked to the interhemispheric contrast of the imposed radiative forcing. When the radiative forcing is stronger in one hemisphere, an anomalous heat exchange between the hemispheres results. This heat exchange is accompanied by an anomalous cross-equatorial Hadley circulation. The magnitude of the interhemispheric heat transport is little sensitive to the forcing agent or the detailed meridional structure of the forcing, and it is about 60% of the radiative forcing contrast in this model. Because the hemisphere with the more positive radiative forcing typically undergoes greater warming, the ITCZ usually, but not always, appears to move toward the warmer hemisphere. One important feedback remaining to be explored is the role of ocean dynamical feedback.

While the efficacy of GHGs other than CO_2 is not investigated in this study, differences from CO_2 have been reported (Hansen et al. 2005; Ponater et al. 2006). Also, efficacy as low as 0.6 was reported for contrails, although their radiative forcing is very small (Ponater et al. 2005, 2006). In addition, there is a large uncertainty in the prescribed ozone and aerosol distributions. Ultimately, this issue can only be adequately addressed by incorporating two-way interactions between climate and aerosol distributions as has been done in other studies (Feichter et al. 2004; Liepert et al. 2004; Roberts and Jones 2004; Wang 2004). A related large source of uncertainty is a lack of the aerosol indirect effect, which could dominate over the combined direct and semidirect effect on a global scale (Lohmann and Feichter 2001, 2005). In addition, the effect of black carbon on snow and ice surface albedo change is not included in the present study. Furthermore, the chemical interaction between ozone and methane, and indirect effect of methane on stratospheric water vapor, could also be important (Hansen et al. 2005). It is clear that further study is needed to quantify the link between forcings and feedback processes thoroughly.

Acknowledgments. We thank Rich Gudgel, who made some of the data used in this study available to us and helped us to run the GCM. We also thank Rick Hemler, who helped us to run the offline radiation code. Discussions with Tom Delworth and V. Ramaswamy were valuable, and constructive comments by two anonymous reviewers are greatly appreciated. Tremendous computational resources have been kindly provided by NOAA/GFDL. The developers of Ferret and NCL are also appreciated. This research was supported by the Climate Change Data and Detection element of the NOAA Climate and Global Change Program under Award number OAR43100107.

REFERENCES

Allen, M. R., and W. J. Ingram, 2002: Constraints on future changes in climate and the hydrologic cycle. *Nature,* **419,** 224–232.

Berntsen, T. K., I. S. A. Isaksen, G. Myhre, J. S. Fuglestvedt, F. Stordal, T. A. Larsen, R. S. Freckleton, and K. P. Shine, 1997: Effects of anthropogenic emissions on tropospheric ozone and its radiative forcing. *J. Geophys. Res.,* **102** (D23), 28 101–28 126.

Betts, A. K., and W. Ridgway, 1989: Climatic equilibrium of the atmospheric convective boundary layer over a tropical ocean. *J. Atmos. Sci.,* **46,** 2621–2641.

Bony, S., and Coauthors, 2006: How well do we understand and evaluate climate change feedback processes? *J. Climate,* **19,** 3445–3482.

Broccoli, A. J., 2000: Tropical cooling at the last glacial maximum: An atmosphere–mixed layer ocean model simulation. *J. Climate,* **13,** 951–976.

——, K. A. Dahl, and R. J. Stouffer, 2006: Response of the ITCZ to Northern Hemisphere cooling. *Geophys. Res. Lett.,* **33,** L01702, doi:10.1029/2005GL024546.

Charlson, R. J., S. E. Schwartz, J. M. Hales, R. D. Cess, J. A. Coakley Jr., J. E. Hansen, and D. J. Hofmann, 1992: Climate forcing by anthropogenic aerosols. *Science,* **255,** 423–430.

Chen, J., B. E. Carlson, and A. D. D. Genio, 2002: Evidence for strengthening of the tropical general circulation in the 1990s. *Science,* **295,** 838–841.

Cheng, Y., U. Lohmann, J. Zhang, Y. Luo, Z. Liu, and G. Lesins, 2005: Contribution of changes in sea surface temperature and aerosol loading to the decreasing precipitation trend in Southern China. *J. Climate,* **18,** 1381–1390.

Chiang, J. C. H., and C. M. Bitz, 2005: Influence of high latitude ice cover on the marine Intertropical Convergence Zone. *Climate Dyn.,* **25,** 477–496.

——, M. Biasutti, and D. S. Battisti, 2003: Sensitivity of the Atlantic Intertropical Convergence Zone to Last Glacial Maximum boundary conditions. *Paleoceanography,* **18,** 1094, doi:10.1029/2003PA000916.

Chung, C. E., V. Ramanathan, and J. T. Kiehl, 2002: Effects of the South Asian absorbing haze on the northeast monsoon and surface-air heat exchange. *J. Climate,* **15,** 2462–2476.

Colman, R., 2003: A comparison of climate feedbacks in general circulation models. *Climate Dyn.,* **20,** 865–873.

——, and B. J. McAvaney, 1997: A study of general circulation model climate feedbacks determined from perturbed sea surface temperature experiments. *J. Geophys. Res.,* **102** (D16), 19 383–19 402.

Cook, J., and E. J. Highwood, 2004: Climate response to tropospheric absorbing aerosols in an intermediate general-circulation model. *Quart. J. Roy. Meteor. Soc.,* **130,** 175–191.

Dahl, K. A., A. J. Broccoli, and R. J. Stouffer, 2005: Assessing the role of the North Atlantic freshwater forcing in millennial scale climate variability: A tropical Atlantic perspective. *Climate Dyn.,* **24,** 325–346.

Delworth, T. L., and Coauthors, 2006: GFDL's CM2 global coupled climate models. Part I: Formulation and simulation characteristics. *J. Climate,* **19,** 643–674.

Feichter, J., E. Roeckner, U. Lohmann, and B. Liepert, 2004: Nonlinear aspects of the climate response to greenhouse gas and aerosol forcing. *J. Climate,* **17,** 2384–2398.

Forster, P. M. F., M. Blackburn, R. Glover, and K. P. Shine, 2000: An examination of climate sensitivity for idealised climate change experiments in an intermediate general circulation model. *Climate Dyn.,* **16,** 833–849.

Genfo, A. D. D., A. A. Lacis, and R. A. Ruedy, 1991: Simulations of the effect of a warmer climate on atmospheric humidity. *Nature,* **351,** 382–385.

GFDL GAMDT, 2004: The new GFDL global atmosphere and land model AM2–LM2: Evaluation with prescribed SST simulations. *J. Climate,* **17,** 4641–4673.

Hansen, J., and M. Sato, 2001: Trends of measured climate forcing agents. *Proc. Natl. Acad. Sci. USA,* **98,** 14 778–14 783.

——, A. Lacis, D. Rind, G. Russel, P. Stone, I. Fung, R. Ruedy, and J. Lerner, 1984: Climate sensitivity: Analysis of feedback mechanisms. *Climate Processes and Climate Sensitivity, Geophys. Monogr.,* Vol. 29, Amer. Geophys. Union, 130–163.

——, M. Sato, and R. Ruedy, 1997a: Radiative forcing and climate response. *J. Geophys. Res.,* **102** (D6), 6831–6864.

——, and Coauthors, 1997b: Forcings and chaos in interannual to decadal climate change. *J. Geophys. Res.,* **102** (D22), 25 679–25 720.

——, and Coauthors, 2005: Efficacy of climate forcings. *J. Geophys. Res.,* **110,** D18104, doi:10.1029/2005JD005776.

Hartmann, D. L., 1994: *Global Physical Climatology*. International Geophysics Series, Vol. 56, Academic Press, 411 pp.

Haywood, J., and O. Boucher, 2000: Estimates of the direct and indirect radiative forcing due to tropospheric aerosols: A review. *Rev. Geophys.,* **38,** 513–543.

Held, I. M., and B. J. Soden, 2000: Water vapor feedback and global warming. *Annu. Rev. Energy Environ.,* **25,** 441–475.

——, and ——, 2006: Robust responses of the hydrological cycle to global warming. *J. Climate,* **19,** 5686–5699.

Horowitz, L. W., and Coauthors, 2003: A global simulation of tropospheric ozone and related tracers: Description and evaluation of MOZART, version 2. *J. Geophys. Res.,* **108,** 4784, doi:10.1029/2002JD002853.

Jackson, C. S., and A. J. Broccoli, 2003: Orbital forcing of Arctic climate: Mechanisms of climate response and implications for continental glaciation. *Climate Dyn.,* **21,** 539–557.

Joshi, M., K. Shine, M. Ponater, N. Stuber, R. Sausen, and L. Li, 2003: A comparison of climate response to different radiative forcings in three general circulation models: Towards an improved metric of climate change. *Climate Dyn.,* **20,** 843–854.

Knutson, T. R., and S. Manabe, 1995: Time-mean response over the tropical Pacific to increased CO_2 in a coupled ocean–atmosphere model. *J. Climate,* **8,** 2181–2199.

——, and Coauthors, 2006: Assessment of twentieth-century regional surface temperature trends using the GFDL CM2 coupled models. *J. Climate,* **19,** 1624–1651.

Lambert, F. H., and N. E. Faull, 2007: Tropospheric adjustment: The response of two general circulation models to a change in insolation. *Geophys. Res. Lett.,* **34,** L03701, doi:10.1029/2006GL028124.

Liepert, B. G., J. Feichter, U. Lohmann, and E. Roeckner, 2004: Can aerosols spin down the water cycle in a warmer and moister world? *Geophys. Res. Lett.,* **31,** L06207, doi:10.1029/2003GL019060.

Lin, S.-J., 2004: A vertically Lagrangian finite-volume dynamical core for global models. *Mon. Wea. Rev.,* **132,** 2293–2307.

Lohmann, U., and J. Feichter, 2001: Can the direct and semi-direct aerosol effect compete with the indirect effect on a global scale? *Geophys. Res. Lett.,* **28** (1), 159–162.

——, and ——, 2005: Global indirect aerosol effect: A review. *Atmos. Chem. Phys.,* **5,** 715–737.

Manabe, S., and R. T. Wetherald, 1967: Thermal equilibrium of the atmosphere with a given distribution of relative humidity. *J. Atmos. Sci.,* **24,** 241–259.

——, and ——, 1975: The effects of doubling the CO_2 concentration on the climate of a general circulation model. *J. Atmos. Sci.,* **32,** 3–15.

Menon, S., J. Hansen, L. Nazarenko, and Y. Luo, 2002: Climate effects of black carbon aerosols in China and India. *Science,* **297,** 2250–2253.

Mickley, L. J., D. J. Jacob, B. D. Field, and D. H. Rind, 2004: Climate response to the increase in tropospheric ozone since preindustrial times: A comparison between ozone and equivalent CO_2 forcings. *J. Geophys. Res.,* **109,** D05106, doi:10.1029/2003JD003653.

Milly, P. C. D., and A. B. Shmakin, 2002: Global modeling of land water and energy balances. Part I: The land dynamics (LaD) model. *J. Hydrometeor.,* **3,** 283–299.

Mitas, C. M., and A. Clement, 2005: Has the Hadley cell been strengthening in recent decades? *Geophys. Res. Lett.,* **32,** L03809, doi:10.1029/2004GL021765.

Moorthi, S., and M. J. Suarez, 1992: Relaxed Arakawa–Schubert: A parameterization of moist convection for general circulation models. *Mon. Wea. Rev.,* **120,** 978–1002.

NRC, Ed., 2005: *Radiative Forcing of Climate Change: Expanding the Concept and Addressing Uncertainties*. The National Academies Press, 224 pp.

Peixoto, J. P., and A. H. Oort, 1992: *Physics of Climate*. American Institute of Physics, 520 pp.

Ponater, M., S. Marquart, R. Sausen, and U. Schumann, 2005: On contrail climate sensitivity. *Geophys. Res. Lett.,* **32,** L10706, doi:10.1029/2005GL022580.

——, S. Pechtl, R. Sausen, U. Schumann, and G. Hüttig, 2006: Potential of the cryoplane technology to reduce aircraft climate impact: A state-of-the-art assessment. *Atmos. Environ.,* **40,** 6928–6944.

Ramanathan, V., P. J. Crutzen, J. T. Keihl, and D. Rosenfeld, 2001: Aerosols, climate, and the hydrological cycle. *Science,* **294,** 2119–2124.

Ramaswamy, V., and C.-T. Chen, 1997: Linear additivity of climate response for combined albedo and greenhouse perturbations. *Geophys. Res. Lett.,* **24** (5), 567–570.

Randel, W. J., and F. Wu, 1999: A stratospheric ozone trends data set for global modeling studies. *Geophys. Res. Lett.,* **26** (20), 3089–3092.

Roberts, D. L., and A. Jones, 2004: Climate sensitivity to black carbon aerosol from fossil fuel combustion. *J. Geophys. Res.,* **109,** D16202, doi:10.1029/2004JD004676.

Rotstayn, L. D., 1997: A physically based scheme for the treatment of stratiform clouds and precipitation in large-scale models. I: Description and evaluation of microphysical processes. *Quart. J. Roy. Meteor. Soc.,* **123** (541), 1227–1282.

——, and U. Lohmann, 2002: Tropical rainfall trends and the indirect aerosol effect. *J. Climate,* **15,** 2103–2116.

Santer, B. D., and Coauthors, 1996: A search for human influences on the thermal structure of the atmosphere. *Nature,* **382,** 39–46.

Schlesinger, M. E., 1988: Quantitative analysis of feedbacks in climate model simulations of CO_2-induced warming. *Physically-Based Modelling and Simulation of Climate and Climatic Change: Part 2,* M. E. Schlesinger, Ed., NATO ASI Series C: Mathematical and Physical Sciences, Vol. 243, Kluwer Academic Publishers, 653–735.

Shindell, D., G. Faluvegi, A. Lacis, J. Hansen, R. Ruedy, and E. Aguilar, 2006: Role of tropospheric ozone increases in 20th-century climate change. *J. Geophys. Res.,* **111,** D08302, doi:10.1029/2005JD006348.

Shine, K. P., J. Cook, E. J. Highwood, and M. M. Joshi, 2003: An alternative to radiative forcing for estimating the relative importance of climate change mechanisms. *Geophys. Res. Lett.,* **30,** 2047, doi:10.1029/2003GL018141.

Soden, B. J., and I. M. Held, 2006: An assessment of climate feedbacks in coupled ocean-atmosphere models. *J. Climate,* **19,** 3354–3360.

——, A. J. Broccoli, and R. S. Hemler, 2004: On the use of cloud forcing to estimate cloud feedback. *J. Climate,* **17,** 3661–3665.

Sokolov, A. P., 2006: Does model sensitivity to changes in CO_2 provide a measure of sensitivity to other forcings? *J. Climate,* **19,** 3294–3306.

Solomon, S., D. Qin, M. Manning, Z. Chen, M. Marquis, K. B. Averyt, M. Tignor, and H. L. Miller, Eds., 2007: *Climate Change 2007: The Physical Science Basis*. Cambridge University Press, 996 pp.

Stainforth, D. A., and Coauthors, 2005: Uncertainty in predictions of the climate response to rising levels of greenhouse gases. *Nature,* **433,** 403–406.

Stenchikov, G. L., I. Kirchner, A. Robock, H.-F. Graf, J. C. Antuña, R. G. Grainger, A. Lambert, and L. Thomason, 1998: Radiative forcing from the 1991 Mount Pinatubo volcanic eruption. *J. Geophys. Res.,* **103** (D12), 13 837–13 858.

Stuber, N., M. Ponater, and R. Sausen, 2001: Is the climate sensitivity to ozone perturbations enhanced by stratospheric water vapor feedback? *Geophys. Res. Lett.,* **28** (15), 2887–2890.

——, M. Ponator, and R. Sausen, 2005: Why radiative forcing might fail as a predictor of climate change. *Climate Dyn.,* **24,** 497–510.

Taylor, K. E., M. Crucifix, P. Braconnot, C. D. Hewitt, C. Doutriaux, A. J. Broccoli, J. F. B. Mitchell, and M. J. Webb, 2007: Estimating shortwave radiative forcing and response in climate models. *J. Climate,* **20,** 2530–2543.

Tett, S. F. B., J. F. B. Mitchell, D. E. Parker, and M. R. Allen, 1996: Human influence on the atmospheric vertical temperature structure: Detection and observations. *Science,* **274,** 1170–1173.

Tiedtke, M., 1993: Representation of clouds in large-scale models. *Mon. Wea. Rev.,* **121,** 3040–3061.

Vecchi, G. A., and B. J. Soden, 2007: Global warming and the weakening of the tropical circulation. *J. Climate,* **20,** 4316–4340.

——, ——, A. T. Wittenberg, I. M. Held, A. Leetma, and M. J. Harrison, 2006: Weakening of tropical Pacific atmospheric circulation due to anthropogenic forcing. *Nature,* **441,** 73–76.

Vellinga, M., and R. A. Wood, 2002: Global climatic impacts of a collapse of the Atlantic thermohaline circulation. *Climatic Change,* **54,** 251–267.

Wang, C., 2004: A modeling study on the climate impacts of black carbon aerosols. *J. Geophys. Res.,* **109,** D03106, doi:10.1029/2003JD004084.

Wentz, F. J., and M. Schabel, 2000: Precise climate monitoring using complementary satellite data sets. *Nature,* **403,** 414–416.

Wetherald, R. T., and S. Manabe, 1975: The effects of changing the solar constant on the climate of a general circulation model. *J. Atmos. Sci.,* **32,** 2044–2059.

——, and ——, 1988: Cloud feedback processes in a general circulation model. *J. Atmos. Sci.,* **45,** 1397–1416.

Wielicki, B. A., and Coauthors, 2002: Evidence for large decadal variability in the tropical mean radiative energy budget. *Science,* **295,** 841–844.

Williams, K. D., A. Jones, D. L. Roberts, C. A. Senior, and M. J. Woodage, 2001: The response of the climate system to the indirect effects of anthropogenic sulfate aerosol. *Climate Dyn.,* **17,** 845–856.

Winton, M., 2000: A reformulated three-layer sea ice model. *J. Atmos. Oceanic Technol.,* **17,** 525–531.

Yokohata, T., S. Emori, T. Nozawa, Y. Tsushima, T. Ogura, and M. Kimoto, 2005a: Climate response to volcanic forcing: Validation of climate sensitivity of a coupled atmosphere-ocean general circulation model. *Geophys. Res. Lett.,* **32,** L21710, doi:10.1029/2005GL023542.

——, ——, ——, ——, ——, and ——, 2005b: A simple scheme for climate feedback analysis. *Geophys. Res. Lett.,* **32,** L19703, doi:10.1029/2005GL023673.

Yoshimori, M., C. C. Raible, T. F. Stocker, and M. Renold, 2006: On the interpretation of low-latitude hydrological proxy records based on Maunder Minimum AOGCM simulations. *Climate Dyn.,* **27,** 493–513.

Zhang, M., and H. Song, 2006: Evidence of deceleration of atmospheric vertical overturning circulation over the tropical Pacific. *Geophys. Res. Lett.,* **33,** L12701, doi:10.1029/2006GL025942.

Zhang, R., and T. L. Delworth, 2005: Simulated tropical response to a substantial weakening of the Atlantic thermohaline circulation. *J. Climate,* **18,** 1853–1860.